Molecular Pharmacology Fast Forward. Published on May 30, 2020 as DOI: 10.1124/mol.119.118448
This article has not been copyedited and formatted. The final version may differ from this version.



**Title**

Kinetic analysis of the early signaling steps of the human chemokine receptor CXCR4.

**Name of authors**

Cristina Perpiñá-Viciano, Ali Işbilir, Aurélien Zarca, Birgit Caspar, Laura E. Kilpatrick, Stephen J. Hill, Martine J. Smit, Martin J. Lohse, Carsten Hoffmann*

*Corresponding author

**Affiliations**

Institute of Molecular Cell Biology, Center for molecular biomedicine (CMB), University Hospital Jena, University of Jena, Hans-Knöll-Str. 2, D-07745, Jena, Germany (CPV, CH)

Institute of Pharmacology and Toxicology, University of Würzburg, Versbacher-Str. 9, 97078 Würzburg, Germany (CPV, CH, AI, MJL)

Max-Delbrück Center for Molecular Medicine, Robert-Rössle-Str. 10, 13125 Berlin, Germany (AI, MJL)

Amsterdam Institute for Molecules Medicines and Systems (AIMMS), Division of Medicinal Chemistry, Vrije Universiteit, De Boelelaan 1108, 1081 HZ, Amsterdam, The Netherlands (AZ, MJS)

Division of Physiology, Pharmacology and Neuroscience, School of Life Sciences, University of Nottingham, Medical School, Queen's Medical Centre, Nottingham, NG7 2UH, U.K (BC, LEK, SJH)

Centre of Membrane Proteins and Receptors (COMPARE), University of Birmingham and University of Nottingham, The Midlands, NG7 2UH, U.K (BC, LEK, SJH)

Molecular Pharmacology Fast Forward. Published on May 30, 2020 as DOI: 10.1124/mol.119.118448
This article has not been copyedited and formatted. The final version may differ from this version.



**Running Title**

Early steps in the activation mechanism of CXCR4

**Corresponding author**

Prof. Dr. Carsten Hoffmann; Institute of Molecular Cell Biology, Center for molecular biomedicine (CMB), University Hospital Jena, University of Jena, Hans-Knöll-Str. 2, D-07745, Jena, Germany; Tel.: 0049 03641/9395600; Fax: 0049 03641/9395602; carsten.hoffmann@med.uni-jena.de

**Text pages:** 46

**Tables:** 0

**Figures:** 8

**References:** 78

**Abstract word count:** 144

**Introduction word count: 756**

**Discussion word count:** 1550

**Abbreviations:**

AR: Adrenergic Receptor; BAL: British Anti-Lewisite; BSA: Bovine Serum Albumin; CD74: Cluster of Differentiation 74; CFP: Cyan Fluorescent Protein; CI: confidence interval; CRE: cAMP-responsive element; CXCL: CXC chemokine Ligand; CXCR: CXC chemokine Receptor; DMEM: Dulbecco's modified eagle medium; DPBS: Dulbecco's Phosphate-Buffered Saline; EDT: 1,2-Ethanedithiol; FlAsH: Fluorescein Arsenical Hairpin binder; FRET: Förster Resonance Energy Transfer; FSK: Forskolin; GPCR: G Protein-Coupled Receptor; HA: Hemagglutinin; HEK293: Human Embryonic Kidney cells 293; HIV: Human Immunodeficiency Virus; ICL: Intracellular Loop; IQR: interquartile range; mGluR: Metabotropic Glutamate Receptors; MIF: Macrophage migration

Molecular Pharmacology Fast Forward. Published on May 30, 2020 as DOI: 10.1124/mol.119.118448
This article has not been copyedited and formatted. The final version may differ from this version.



Inhibitory Factor; NLuc: NanoLuc; PEI: polyethylenimine; PTH: Parathyroid Hormone; PTHR1: Parathyroid Hormone Receptor 1; SD: Standard Deviation; SEM: Standard Error of the Mean; TM: Trans-membrane; WT: wild-type; YFP: Yellow Fluorescent Protein; 5HT: 5-Hydroxytryptamine or serotonin.

Molecular Pharmacology Fast Forward. Published on May 30, 2020 as DOI: 10.1124/mol.119.118448
This article has not been copyedited and formatted. The final version may differ from this version.



**Abstract**

G protein-coupled receptors (GPCRs) are biological switches that transduce extracellular stimuli into intracellular responses in the cell. Temporally resolving GPCR transduction pathways is key to understanding how cell signaling occurs. Here, we investigate the kinetics and dynamics of the activation and early signaling steps of the chemokine receptor CXCR4 in response to its natural ligands CXCL12 and macrophage migration inhibitory factor (MIF), using Förster resonance energy transfer-based approaches. We show that CXCR4 presents a multifaceted response to CXCL12, with receptor activation (≈0.6s) followed by a rearrangement in the receptor/G protein complex (≈1s), a slower dimer rearrangement (≈1.7s) and prolonged G protein activation (≈4s). In comparison, MIF distinctly modulates every step of the transduction pathway, indicating distinct activation mechanisms and reflecting the different pharmacological properties of these two ligands. Our study also indicates that CXCR4 exhibits some degree of ligand-independent activity, a relevant feature for drug development.

Molecular Pharmacology Fast Forward. Published on May 30, 2020 as DOI: 10.1124/mol.119.118448
This article has not been copyedited and formatted. The final version may differ from this version.



**Significance statement**

The CXCL12/CXCR4 axis represents a well-established therapeutic target for cancer treatment. We demonstrate that CXCR4 exhibits a multifaceted response that involves dynamic receptor dimer rearrangements, which is kinetically embedded between receptor-G protein complex rearrangements and G protein activation. The alternative endogenous ligand MIF behaves opposite to CXCL12 in each assay studied and does not lead to G protein activation. This detailed understanding of the receptor activation may aid in the development of more specific drugs against this target.

Molecular Pharmacology Fast Forward. Published on May 30, 2020 as DOI: 10.1124/mol.119.118448
This article has not been copyedited and formatted. The final version may differ from this version.



## Introduction

G protein-coupled receptors (GPCRs) transduce signals of diverse nature from the extracellular side into specific responses within the cell through a succession of biochemical events. Generally, binding of an agonist to a receptor causes structural changes in the transmembrane (TM) helices that stabilize the receptor in an active conformation. This is followed by interaction with and subsequent activation of heterotrimeric G proteins, which modulate the activity of different downstream effectors. Receptors can then be phosphorylated by kinases and internalized, resulting in degradation or recycling to the plasma membrane (Hilger et al., 2018).

Crystal structure analysis has provided enormous insights into the molecular mechanisms involved in GPCR activation. However, the detailed temporal dynamics of these changes cannot be resolved in these studies. In this aspect, the use of Förster resonance energy transfer (FRET)-based approaches represent a tool to investigate the dynamics and kinetics of GPCR activation and their downstream signaling events in real time and in intact cells (Lohse et al., 2012). The most common structural characteristic of receptor activation is a large outward shift of the intracellular part of TM domain VI (Altenbach et al., 2008). This unique feature has been the basis for the development of FRET sensors for many receptors, which can report ligand-induced structural rearrangements in a temporal manner (Lohse et al., 2014; Stumpf and Hoffmann, 2016; Wright et al., 2018). These sensors together with other FRET-based approaches have helped to understand the distinct mechanisms of activation between different ligand types (Vilardaga et al., 2005), allosterism (Messerer et al., 2017), and receptor classes (Vilardaga et al., 2003). Most studies have found activation time constants of monomeric GPCRs on the order of 30-50 ms (Hoffmann et al., 2005; Rochais et al., 2007; Reiner et al., 2010; Ziegler et al., 2011). However, there are apparent differences between various receptor types. Thus, activation of class B parathyroid hormone receptor 1 (PTHR1) by its large agonist PTH(1-34) is about 20-fold slower (Vilardaga et al., 2003). Another specific case is the activation in dimeric receptors. In a recent study aiming at resolving rapid activation steps of metabotropic glutamate receptors (mGluR), it was shown that an initial rearrangement of the dimer structure occurs within 1-2 ms, while conformational changes in the 7-helix TM structure occur within 20 ms

Molecular Pharmacology Fast Forward. Published on May 30, 2020 as DOI: 10.1124/mol.119.118448
This article has not been copyedited and formatted. The final version may differ from this version.



(Grushevskyi et al., 2019). Another open question regarding activation in receptor dimers is how the two protomers influence each other. An early study of $\alpha_2$-adrenergic/μ-opioid heterodimers suggested that in such a dimer only one of the two protomers is active (Vilardaga et al., 2008). Likewise, initial studies of mGluRs indicated that only one of the two protomers becomes activated (Hlavackova et al., 2005). However, it now appears clear that activation of both protomers is required for full activation (Kniazeff et al., 2004; Grushevskyi et al., 2019).

The CXC chemokine receptor 4 (CXCR4) appears to be a facultative homodimer, and dimer formation may contribute to its signaling function. CXCR4 and its cognate ligand CXCL12, formerly known as stromal cell-derived factor-1, are key players in cell migration in different contexts (Alsayed et al., 2007; Yang et al., 2013). A two-step binding mechanism of chemokines to their chemokine receptors has been proposed (Qin et al., 2015). Binding of CXCL12 preferentially results in activation of $G_i$ proteins as well as β-arrestin recruitment (Heuninck et al., 2019). The CXCR4/CXCL12 axis is an important therapeutic target for the development of new drugs due to its involvement in several types of cancer (Guo et al., 2016; Adlere et al., 2019; Bobkov et al., 2019), in addition to the well-proven role of CXCR4 as a HIV co-receptor (Tsibris and Kuritzkes, 2007). Recently, macrophage migration inhibitory factor (MIF) has also been demonstrated to bind to CXCR4, but the binding mode and downstream consequences observed greatly differ from those of CXCL12. For instance, MIF binding to the receptor does not result in β-arrestin recruitment (Bernhagen et al., 2007; Rajasekaran et al., 2016; Lacy et al., 2018). The biomedical importance of CXCR4 and its ligands, their dynamic monomer/dimer equilibrium, the suggested two-step activation mechanism and the existence of several endogenous agonists with diverse effects all make the spatio-temporal analysis of CXCR4 signaling particularly interesting.

Therefore, we set out to analyze the early steps of CXCR4 activation in response to the two distinct ligands CXCL12 and MIF. We have combined several FRET approaches to elucidate the temporal aspects of the receptor-mediated early signaling events with sub-second resolution. Our data show that these two ligands modulate the receptor's activity oppositely and that, in the absence of agonist, CXCR4 exhibits some degree of constitutive activity.

Molecular Pharmacology Fast Forward. Published on May 30, 2020 as DOI: 10.1124/mol.119.118448
This article has not been copyedited and formatted. The final version may differ from this version.



## Materials and Methods

### Plasmid DNA constructs

Human CXCR4 with YFP fused to the C-terminus was a kind gift of F. Bachelerie (INSERM, Université Paris-Sud, France; Levoye et al., 2009). The $\alpha_{2A}$-adrenergic receptor (AR) has been previously described (Bünemann et al., 2003). The G protein subunits $G\alpha_{i1}$, $G\alpha_{i1}$-CFP, $G\beta_1$, $G\gamma_2$ and $G\gamma_2$-CFP and the $\alpha_{2A}$-AR-YFP (labeled at the C-terminus) have been previously described (Hein et al., 2005). The G protein sensors for $G_{i1}$, $G_{i2}$, $G_{i3}$ and $G_q$ have been previously described (Adjobo-Hermans et al., 2011; Van Unen et al., 2016). The cAMP-responsive element (CRE)-Luc construct has been previously described (Watts et al., 2013)

Human CXCR4 and human CXCR4 with three hemagglutinin (HA) tags fused to the N-terminus (3HA-CXCR4) are in pcDEF3 (Vrije Universiteit, Amsterdam, The Netherlands). The 3HA-CXCR4 construct was employed to label the receptor with enhanced CFP (BD Biosciences). For that, the fluorescent protein was fused in-frame to the C-terminus of CXCR4 by standard PCR extension overlap technique. The C-terminal stop codon of the receptor and the initial methionine codon of the fluorescent protein were deleted. The resulting construct was named CXCR4-CFP and contains the fluorescent protein following S352. To create the different receptor sensors, the FlAsH-binding motif CCPGCC was inserted at different positions within the intracellular loop-3 (ICL-3) of the receptor in the CXCR4-CFP construct: between amino acids L226 and S227 (CXCR4-FlAsH226-CFP), between amino acids H228 and S229 (CXCR4-FlAsH228-CFP), or between amino acids S229 and K230 (CXCR4-FlAsH229-CFP). Cloning was performed using site-directed mutagenesis by overlap extension PCR. To create analogous constructs only containing the FlAsH-binding motif in different positions of ICL-3 (CXCR4-FlAsH226, CXCR4-FlAsH228 and CXCR4-FlAsH229), the CFP was removed from the C-terminus of the corresponding receptor sensors via standard PCR.

The Pfu polymerase was used for amplifying DNA in the PCRs, and the T4 ligase enzyme was used for ligation. *Escherichia coli* DH5α (Invitrogen) was used as a host to clone all the genes described. All constructs were verified by sequencing (Eurofins Genomix GmbH, Germany).

Molecular Pharmacology Fast Forward. Published on May 30, 2020 as DOI: 10.1124/mol.119.118448
This article has not been copyedited and formatted. The final version may differ from this version.



**Ligands**

Recombinant human CXCL12 was purchased from Peprotech (#300-28A); Recombinant human MIF was purchased from Peprotech (#300-69); Norepinephrine was purchased from Sigma Aldrich (#A9512); IT1t was purchased from Tocris (#4596). AMD3100 was purchased from Sigma Aldrich (A5602); CXCL12-AlexaFluor647 is from Almac (CAF-11).

**Cell lines and cell culture**

Human embryonic kidney 293 (HEK293 and HEK293T) cell lines (ATCC; CRL-1573 and CRL-3216) were cultured using Dulbecco's Modified Eagle Medium (DMEM) supplemented with 4.5 g/l glucose (Gibco), 10% (v/v) fetal bovine serum (Biochrom), 1% penicillin/streptomycin (Gibco) and 1% L-glutamine (PanBiotech). Cells were kept in a humidified 7% $CO_2$ atmosphere at 37°C. For routine maintenance, cells were split every two or three days by rinsing them with Dulbecco's Phosphate-Buffered Saline (DPBS; Gibco) and, then, trypsin-EDTA (PanBiotech). Cell lines were routinely tested for mycoplasma contamination by PCR using a primer set specific for the highly conserved 16S rRNA coding region in the mycoplasma genome. Cells have not been authenticated.

The N-terminal NanoLuc (NLuc)-labeled CXCR4 receptor construct was created from a previously described construct (Stoddart et al., 2015) and was used for the binding competition assay. Briefly, the adenosine $A_1$ receptor cDNA was replaced with that encoding the human CXCR4 (NM_003467.2). The resultant construct fused NLuc in-frame with the membrane signal sequence from the 5-$HT_{3A}$ receptor within pcDNA3.1 to generate signal-NLuc. The human CXCR4 sequence (methionine start signal removed) was then fused to the 3' end of signal-NLuc via a short Gly-Ser linker. Stable mixed expression populations of HEK293G cell lines (HEK293 expressing the GloSensor™ (20F) cAMP biosensor; Promega Corporation) expressing the NLuc-CXCR4 cDNA construct were created by transfecting cells with FuGENE HD (Promega Corporation) following the manufacturer's instructions. Cells were then subject to antibiotic selection using G418 disulfate salt (1mg/ml; Sigma Aldrich) for 2-3 weeks, screened for luminescence expression and expanded. The HEK293G-NLuc-CXCR4 cell line was cultured using DMEM (Sigma Aldrich) supplemented with 10% fetal bovine serum (Sigma

Molecular Pharmacology Fast Forward. Published on May 30, 2020 as DOI: 10.1124/mol.119.118448
This article has not been copyedited and formatted. The final version may differ from this version.



Aldrich). Cells were kept in a humidified 5% $CO_2$ atmosphere at 37°C. For routine maintenance, cells were split every two or three days by using DPBS (Lonza) and trypsin-EDTA (0.25% w/v versene; Lonza).

**FlAsH labeling**

FlAsH labeling was done as previously described (Hoffmann et al., 2010) right before the measurements. In brief, transfected cells grown on 24 mm glass coverslips (Hartenstein, Würzburg, Germany) or 40 mm WillCo dishes (WillCo Wells) were washed twice with labeling buffer (150 mM NaCl, 10 mM HEPES, 2.5 mM KCl, 4 mM $CaCl_2$, 2 mM $MgCl_2$ freshly supplemented with 1.8 g/l glucose; pH 7.3). Subsequently, cells were incubated for 1h at 37°C with labeling buffer containing 1 µM FlAsH (commercially available from Thermo Fisher Scientific, Darmstadt, Germany as TC-FlAsH labeling kit) and 12.5 µM 1,2-ethanedithiol (EDT; Sigma Aldrich). Cells were rinsed twice and incubated for 10 min at 37°C in labeling buffer containing 250 µM EDT to reduce non-specific FlAsH labeling. Finally, cells were washed twice and kept in media at 37°C until measurement.

**Confocal microscopy**

HEK293 cells were seeded on 24 mm glass coverslips, which had been previously coated with poly-D-lysine (1 mg/ml; MP Biomedicals) for 30 min and washed once with DPBS, placed in wells of a 6-well plate. After 6h and for each well, cells were transfected with 0.5 µg of the different CXCR4 sensors (CXCR4-FlAsH226-CFP, CXCR4-FlAsH228-CFP or CXCR4-FlAsH229-CFP) using Effectene (Qiagen), following the manufacturer's instructions. Prior to transfection, the media of the cells was exchanged for fresh media. Cells were analyzed 48h after transfection. When indicated, cells were FlAsH-labeled right before the measurement. During the experiment, cells were kept in imaging buffer (140 mM NaCl, 5.4 mM KCl, 2 mM $CaCl_2$, 1 mM $MgCl_2$, 10 mM HEPES; pH 7.3).

Confocal microscopy was performed using a Leica TCS SP8 system (Leica Microsystems, Germany) with an Attofluor holder (Molecular Probes) and images were taken with a 63× water objective (numerical aperture 1.4). CFP was excited with a diode laser line at 442 nm and fluorescence

Molecular Pharmacology Fast Forward. Published on May 30, 2020 as DOI: 10.1124/mol.119.118448
This article has not been copyedited and formatted. The final version may differ from this version.



intensities were recorded from 470 to 550 nm. FlAsH was excited with an argon laser line at 514 nm and fluorescence intensities were recorded from 525 to 600 nm. Images were acquired at 1024×1024 pixel format, line average 3 and 400 Hz. To avoid bleed through, parallel images of CFP and FlAsH were taken in sequential scan. Images were analyzed using the Leica Application Suite Advanced Fluorescence Software (Leica Microsystems, Germany).

**Single-cell FRET experiments**

Microscopic FRET set-up

FRET measurements were performed on an inverted microscope (Zeiss Axiovert 200, Zeiss) equipped with an oil immersion 63x objective lens and a dual-emission photometric system (Till Photonics). The transfected cells were excited with light from a polychrome IV (Till Photonics) at a frequency of 10 Hz with 40 ms illumination out of a total time of 100 ms. Emission of the donor (CFP or mTurquoise2; 480 ± 20 nm) and acceptor (YFP, FlAsH or Venus; 535 ± 15 nm), and the FRET ratio (Facceptor/Fdonor) were monitored simultaneously (beam splitter DCLP 505 nm) upon excitation at 436 ± 10 nm (beam splitter DCLP 460 nm). Fluorescence signals were detected by photodiodes, digitalized using an analogue-digital converter (Digidata 1440A, Axon Instruments) and stored with Clampex 9.0 software (Molecular Devices, Sunnyvale, CA).

Determination of FRET efficiency

Determination of the FRET efficiency was performed as previously described (Jost et al., 2008). HEK293 cells were prepared in 24 mm glass coverslips, as described for confocal microscopy. To study the basal intramolecular FRET, cells were transfected with 0.5 µg of CXCR4-FlAsH226-CFP, CXCR4-FlAsH228-CFP or CXCR4-FlAsH229-CFP sensor, per well. To study the basal intermolecular FRET, cells were transfected with 0.3 µg of CXCR4-CFP and 0.3 µg of CXCR4-FlAsH228, per well. Transfection was performed using Effectene. Prior to the measurement, cells were FlAsH-labeled. Then, the coverslips were mounted on an Attofluor holder and kept in 999 µl of imaging buffer. During the measurement (after approximately 30s of recording), 1 µl of British Anti-

Molecular Pharmacology Fast Forward. Published on May 30, 2020 as DOI: 10.1124/mol.119.118448
This article has not been copyedited and formatted. The final version may differ from this version.



Lewisite (BAL; Fluka) was added to yield a final BAL concentration of 5 mM, which displaces FlAsH from its binding site in the receptors' ICL-3. The FRET efficiency was calculated by analyzing the increase in the CFP emission (FCFP) due to dequenching using the formula ($FCFP_{max}$-$FCFP_{min}$)/$FCFP_{max}$ and the Clampfit software (Molecular Devices, Sunnyvale, CA). Data are shown as a scatter plot with mean and standard deviation (SD), in which each dot represents an individual cell. At least three independent repeats were performed for each condition. Measurements were performed using the microscopic FRET set-up described above.

Kinetic measurements

For kinetic experiments, HEK293 cells were seeded on 40 mm WillCo dishes previously coated with poly-D-lysine for 30 min and washed once with DPBS. 6h later, cells were transfected with the appropriate construct(s) using Effectene. For measuring receptor activation, 0.7 µg of each sensor (CXCR4-FlAsH226-CFP, CXCR4-FlAsH228-CFP or CXCR4-FlAsH229-CFP) were transfected per dish and FlAsH labeling was performed before the measurement. For receptor/G protein interaction studies, 0.6 µg of CXCR4-YFP, 0.7 µg of $G\alpha_{i1}$, 0.3 µg of $G\beta_1$ and 0.2 µg of $G\gamma_2$-CFP were transfected per dish. When indicated, 0.6 µg of CXCR4-YFP, 0.7 µg of $G\alpha_{i1}$-CFP, 0.3 µg of $G\beta_1$ and 0.2 µg of $G\gamma_2$ were transfected instead. For measuring G protein activation, 0.4 µg of receptor (CXCR4 or $\alpha_{2A}$-AR) or empty plasmid and 0.75 µg of G protein sensor ($G_{i1}$, $G_{i2}$ or $G_{i3}$) were transfected per dish. For measuring rearrangements within dimers, 0.5 µg of CXCR4-CFP and 0.5 µg of CXCR4-YFP were transfected per dish. Prior to transfection, the media of the cells was exchanged for fresh media. FRET measurements were performed 48h after transfection using the microscopic FRET set-up.

During the experiments, cells were kept in imaging buffer. Then, using the BioPen® microfluidic system (Fluicell, Gothenburg, Sweden; Ainla et al., 2010; Ainla et al., 2012; Wright et al., 2018), single cells were exposed to the different solutions, as follows: cells were initially washed (approximately for 10-20s) with imaging buffer to establish a baseline. Then, cells were stimulated with buffer supplemented with the appropriate ligand (CXCL12, MIF or norepinephrine) at the indicated concentrations in the figures, until the response reached a plateau. Then, cells were washed again with imaging buffer, ideally, until reversal of the ligand-induced signal was observed (return to

Molecular Pharmacology Fast Forward. Published on May 30, 2020 as DOI: 10.1124/mol.119.118448
This article has not been copyedited and formatted. The final version may differ from this version.



baseline). When indicated, a second stimulation and wash-out was performed. The duration of the stimuli is indicated in the figures as horizontal black lines. All the solutions contained 0.1% bovine serum albumin (BSA; AppliChem).

For determining the kinetics of each process (τ values; apparent on- or off-rate), the FRET ratio of individual experiments was fitted to a one component exponential decay function using the Clampfit software. For each case, τ values are shown as a scatter plot with median and interquartile range (IQR), where N is the total number of individual cells measured in several independent experiments, as indicated in the figure legends. When required, statistical significance was tested using Mann-Whitney test or Kruskal-Wallis test. For determining the amplitude of the signals, maximum and minimum values were considered, and data are reported as mean ± SEM.

The emission of the acceptor fluorophores was corrected for that attributable to bleed-through (spillover of donor into the 535 nm channel) and direct excitation (acceptor emission at 436 nm excitation). FRET was normalized and corrected for photobleaching. Processing of the data was done with OriginPro 2016 (OriginLab Corporation, Northampton, MA).

Acceptor photobleaching experiments

HEK293 cells were prepared in 24 mm glass coverslips as previously described for confocal microscopy. 6h later, cells were transfected with 0.6 µg of CXCR4-YFP or $\alpha_{2A}$-AR-YFP, 0.7 µg of $G\alpha_{i1}$, 0.3 µg of $G\beta_1$ and 0.2 µg of $G\gamma_2$-CFP, per dish, using Effectene. Prior to transfection, the media of the cells was exchanged for fresh media. FRET measurements were performed 48h after transfection using the microscopic FRET set-up. For the experiment, CFP and YFP fluorescence intensities were measured at 10 Hz for 40 s with 20 ms illumination out of a total time of 100 ms. Then, the donor was photobleached by illuminating for 9 min at 490 nm with 90 ms illumination out of a total time of 100 ms. Subsequently, the CFP and YFP fluorescence intensities were measured again for 40s with 20ms illumination out of a total time of 100ms. During the measurements, cells were kept in 600 µl of imaging buffer. When indicated, cells expressing CXCR4 and the G protein subunits were pre-treated with media containing 10 µM IT1t for 4h and kept in 600 µl imaging buffer

Molecular Pharmacology Fast Forward. Published on May 30, 2020 as DOI: 10.1124/mol.119.118448
This article has not been copyedited and formatted. The final version may differ from this version.



containing 10 µM IT1t during the measurement. The change in the CFP fluorescence (FCFP) was calculated by considering the values of CFP fluorescence right before and after the bleaching process, using the formula $((FCFP_{after}-FCFP_{before})/FCFP_{after})$ and the Clampfit software. For each condition, three independent repeats were performed. Data are shown as a box plot in which the whiskers represent maximum and minimum values. Statistical significance between groups was tested using unpaired t-test.

**Cre-Luc reporter-gene assay**

The signaling properties of the different CXCR4 constructs were characterized using a CRE-driven reporter gene assay. HEK293T cells were transfected with the CXCR4 constructs (CXCR4, CXCR4-CFP or CXCR4-FlAsH228-CFP) and the CRE-Luc construct using 25 kDa linear polyethylenimine (PEI; Polysciences) as DNA carrier agent in a 1:10 ratio (DNA/PEI). For transfection, 2 µg of DNA were combined with 12 µg of PEI in a total volume of 250 µl 150 mM NaCl and incubated for 20 min at room temperature. Then, 1 million resuspended cells were added to the DNA/PEI mix, and 80 µl were seeded at a density of 32,000 cells/well in a white, flat-bottom 96-well plate (Greiner Bio One). Analysis was done 24h after seeding the cells using Mithras LB940 (Berthold Technologies).

The day of the measurement, cells were incubated in media or media supplemented with 1 µM forskolin (FSK; LC Laboratories) and increasing concentrations of CXCL12 (as indicated in the figure) and incubated for 6h at 37°C. Subsequently, the media was substituted for 25 µl of luciferase assay reagent (45 mM Tris $H_3PO_4$ pH 7.8, 45% glycerol, 3% Triton X-100, 1 mM DTT, 20 mM $MgCl_2$, 800 µM D-Luciferin (Duchefa), 80 µM ATP) and incubated 20 min in the dark. Finally, the plate luminescence was measured and quantified.

The data from concentration-response curves were fitted to a three-parameter sigmoidal model using GraphPad. For each construct tested, four independent experiments were performed in quadruplicate. Means of $EC_{50}$ values and asymmetric 95% confidence interval (CI) are reported in the text and have been calculated based on the logarithmic values ($logEC_{50}$).

Molecular Pharmacology Fast Forward. Published on May 30, 2020 as DOI: 10.1124/mol.119.118448
This article has not been copyedited and formatted. The final version may differ from this version.



**Binding competition assay**

24h prior to assay, HEK293G cells stably expressing NLuc-CXCR4 were seeded on poly-D-lysine coated white flat-bottom 96-well plates at a density of 40,000 cells/well. On the day of the assay, plating medium was removed and replaced with HBSS/0.1% protease free BSA (HBSS composition 10 mM HEPES, 146 mM NaCl, 5 mM KCl, 1 mM $MgS0_4$, 2 mM sodium pyruvate, 1.3 mM $CaCl_2$ and 1.5 mM $NaHCO_3$; pH 7.4 with the addition of 10 mM glucose following autoclaving). A fixed concentration of the fluorescent ligand CXCL12-AlexaFluor647 (10 nM) was added simultaneously in triplicate wells, alongside increasing concentrations of unlabeled CXCL12, AMD3100 or MIF for 120 min at 37°C. The NLuc substrate was then added (50x dilution) and plates left to equilibrate in the dark for 5 min.

Sequential dual luminescence and fluorescence readings were recorded using a PHERAstar FS plate reader (BMG Labtech, Germany) with 460 nm (80 nm bandpass; donor NLuc emission) and >610 nm longpass filters (acceptor CXCL12-AF647 emission). Raw BRET ratios were calculated from the ratio of acceptor to donor emission values. Data were fitted to a three-parameter sigmoidal model using GraphPad. Data were pooled from 5/6 independent experiments (6 independent experiments with CXCL12 and MIF ligands of which 5 experiments also used AMD3100) and are expressed as mean ± SEM.

**G protein activation in 96-well plates**

HEK293T cells were seeded in 100 mm plates and grown until they reached 60-65% confluency. Then, cells were transfected with 1.5 µg of receptor (CXCR4, CXCR4-FlAsH226, CXCR4-FlAsH228 or CXCR4-FlAsH229) and 3 µg of FRET-based G protein sensor ($G_{i1}$, $G_{i2}$, $G_{i3}$, or $G_q$) plasmid using Effectene. When indicated, empty plasmid was transfected instead of receptor. Prior to transfection, the media of the cells was replaced by fresh media. 24h after transfection, cells were harvested in culture media and seeded at a density of 30,000 cells/well in black flat-bottom 96-well plates (Brand). The plates had been preincubated with poly-D-lysine (1 mg/ml) for 30 min and washed once with DPBS. Analysis was done 24h after seeding the cells.

Molecular Pharmacology Fast Forward. Published on May 30, 2020 as DOI: 10.1124/mol.119.118448
This article has not been copyedited and formatted. The final version may differ from this version.



To generate concentration-response curves in a microplate reader, cells were incubated at 37°C during 30 min with 90 µl of imaging buffer containing 0.1% BSA. Afterwards, the fluorescence was read for 5 min to determine the pre-read signal. Following the reading, 10 µl of buffer or increasing concentrations of CXCL12 (indicated in the figure) were added to the wells for a total assay volume of 100 µl. Fluorescence was read again for 20 min to determine the post-read signal. During the measurement, cells were kept at 37°C. CXCL12 was prepared in imaging buffer containing 0.1% BSA. The FRET change produced by each concentration of ligand tested was corrected for the signal obtained in vehicle (non-ligand; buffer)-treated cells. To determine the $EC_{50}$ values for G protein activation, data were fitted to a three-parameter sigmoidal model using GraphPad. N=5 independent experiments performed in quadruplicate. Means of $EC_{50}$ values and asymmetric 95% CI are reported in the text and have been calculated based on the logarithmic values ($logEC_{50}$). Statistical significance was tested using one-way ANOVA followed by Tukey's test on the $logEC_{50}$ values.

To investigate basal G protein activity, HEK293T cells transfected with CXCR4 and the $G_{i2}$ sensor were seeded at a density of 15,000 cells/well following the same protocol as described above for concentration-response curves. Three different conditions were analyzed in parallel: (i) buffer, (ii) IT1t treatment, and (iii) CXCL12 treatment. For (i), cells were incubated with 100 µl of imaging buffer for 4h. For (ii), cells were incubated with 100 µl of imaging buffer supplemented with 100 µM IT1t for 4h. For (iii), cells were incubated with 90 µl of imaging buffer during 4h, and 2 min before the measurement, 10 µl of 1 µM CXCL12 were added (final CXCL12 concentration: 100 nM). All the solutions contained 0.1% BSA. After the treatments, fluorescence was read for 8 min. The FRET detected under the three different conditions was normalized to "buffer treatment", which was set to 100. Three independent repeats were performed in quadruplicate. Data are shown as a bar graph with SD. Statistical significance between groups was tested using unpaired t-test.

Experiments were performed using Synergy™ Neo2 Multi-Mode Microplate Reader (Biotek) with Gen5™ Data Analysis Software. During the measurements, cells were excited at 420/50 nm (Biotek CFP-YFP Filter; 1035013) and emission was monitored at 485/20 nm and 540/25 nm (Biotek CFP-YFP Filter; 1035043).

Molecular Pharmacology Fast Forward. Published on May 30, 2020 as DOI: 10.1124/mol.119.118448
This article has not been copyedited and formatted. The final version may differ from this version.



**Quantification and statistical analysis**

Statistical analyses were performed using GraphPad Prism software (version 7). The statistical tests applied can be found in the figure legends and methods section. When normal distribution can be assumed, t-test or ANOVA followed by Tukey's test were performed. When normal distribution cannot be assumed, Mann-Whitney test or Kruskal-Wallis test were performed. The minimum criterion for statistical significance was p*0.05. It should be noted that due to the exploratory nature of our research, the p-values reported are descriptive and should not be interpreted as hypothesis-testing.

Molecular Pharmacology Fast Forward. Published on May 30, 2020 as DOI: 10.1124/mol.119.118448
This article has not been copyedited and formatted. The final version may differ from this version.



## Results

### Development and functional characterization of FRET-based CXCR4 sensors.

In order to study the conformational movements that CXCR4 undergoes during ligand-induced activation, we generated three different FRET sensors for CXCR4 with modifications in different positions. Addition of FRET-compatible fluorescent proteins or tags into the C-terminus and intracellular loops has been established before in several GPCRs to investigate their activation (Stumpf and Hoffmann, 2016). Conformational changes induced upon ligand binding alter the distance and/or orientation between the fluorophores, resulting in changes in FRET that can be monitored in real time (**Figure 1A**). Therefore, a cyan fluorescent protein (CFP) was fused to the C-terminal end of CXCR4 and the short fluorescein arsenical hairpin binder (FlAsH)-binding motif CCPGCC was inserted in three different positions within the ICL-3: between L226 and S227 to generate the CXCR4-FlAsH226-CFP sensor, between H228 and S229 to generate the CXCR4-FlAsH228-CFP sensor, or between S229 and K230 to generate the CXCR4-FlAsH229-CFP sensor. The receptor constructs were characterized for correct functional properties. In particular, the CXCR4-FlAsH228-CFP sensor was chosen for full characterization, since it produced the highest FRET change upon agonist binding, as shown in the following section. Analysis by confocal microscopy showed that all three CXCR4 sensors localized to the plasma membrane (**Figure 1B upper panel and S1A**). Besides, we observed that FlAsH specifically binds to the FlAsH-binding motif in ICL-3 (**Figure 1B lower panel**), as previously reported for analogous receptor sensors (Hoffmann et al., 2005; Hoffmann et al., 2010).

To investigate intramolecular FRET in the sensors, we performed acceptor bleaching experiments using British Anti-Lewisite (BAL; 2,3-dimercapto-1-propanol) in cells transfected with the sensors and FlAsH-labeled prior to the measurement. BAL displays very high affinity for arsenicals and, at high concentrations, displaces FlAsH from its binding site. Addition of 5 mM BAL led to a decrease in the FlAsH signal and dequenched CFP, proving the existence of basal intramolecular FRET (**Figure S2A**). FRET efficiency was calculated based on the increase in the CFP emission and was determined to be 12.0 ± 3.0 % (mean ± SD) for the CXCR4-FlAsH228-CFP sensor (**Figures 1C**). The constructs

Molecular Pharmacology Fast Forward. Published on May 30, 2020 as DOI: 10.1124/mol.119.118448
This article has not been copyedited and formatted. The final version may differ from this version.



CXCR4-FlAsH226-CFP and CXCR4-FlAsH229-CFP showed FRET efficiencies of 5.0 ± 2.7 % and 16.5 ± 4.3 %, respectively (**Figure S1B**). No basal intermolecular FRET was detected in cells co-expressing CXCR4-CFP and CXCR4-FlAsH228 (**Figure S2B**), which indicates that the observed signal results from intramolecular FRET, and not from cross-talk between adjacent receptors or between protomers of a dimer.

We then characterized the constructs for their ability to induce G protein signaling in response to CXCL12, since they contain the FlAsH-binding sequence in ICL-3, a region generally known to be important for G protein interaction (Hu et al., 2010; Chung, 2013). For this purpose, we used a FRET-based $G_{i1}$ sensor that measures G protein activation as a change in FRET between the labeled Gα and Gγ subunits (van Unen et al., 2016). HEK293 cells co-transfected with the $G_{i1}$ sensor and either CXCR4 or CXCR4-FlAsH228 were stimulated with increasing concentrations of CXCL12 in a 96-well plate assay format. Results showed that CXCR4-FlAsH228 preserves the ability to activate $G_{i1}$ ($EC_{50}$ = 15.5 [9.3-25.9] nM; mean and asymmetric 95% CI) although with lower potency than the wild-type (wt) receptor ($EC_{50}$ = 3.4 [2.3-4.9] nM; **Figure 1D**). The CXCR4-FlAsH226 and CXCR4-FlAsH229 constructs also activated $G_{i1}$ with very similar potencies to CXCR4-FlAsH228 ($EC_{50}$ = 18.1 [5.3-62.2] nM and 17.1 [4.9-59.3] nM, respectively; **Figure S1C**). Subsequently, and in order to examine the functionality of the complete sensor, we assessed the capacity of CXCL12 to inhibit FSK-induced cAMP accumulation in cells expressing CXCR4-FlAsH228-CFP, in comparison to cells expressing CXCR4-CFP or the wt receptor. The results showed that cells expressing the sensor exhibited lower potency for the inhibition of FSK-induced cAMP production ($EC_{50}$ = 19.0 [3.5-102.7] nM) in comparison to the wt ($EC_{50}$ = 2.2 [0.6-8.0] nM). We also noted that the presence of CFP at the end of the C-terminus contributes to an intermediate potency of the sensor with regards to $G_i$ signaling ($EC_{50}$ = 10.6 [1.9-57.9] nM) (**Figure 1E**). Most importantly, the maximal activity of the sensor was comparable to the wt receptor. On the basis of this validation, these three constructs can serve as sensors to monitor ligand-induced intramolecular conformational changes.

**The FRET-based CXCR4 sensors report the dynamics and kinetics of receptor activation and deactivation.**

Molecular Pharmacology Fast Forward. Published on May 30, 2020 as DOI: 10.1124/mol.119.118448
This article has not been copyedited and formatted. The final version may differ from this version.



The CXCR4 sensors were used for further FRET experiments in single cells. In order to investigate the conformational changes upon receptor activation, HEK293 cells transiently expressing the receptor sensors and FlAsH-labeled prior to the measurements were stimulated with 30 μM CXCL12. A saturating concentration of ligand is required to determine the maximal and fastest kinetics of the process as well as to ensure that ligand diffusion to receptors is not time-limiting. A BioPen® microfluidic device (Fluicell, Gothenburg, Sweden) was employed for delivering the solutions. This perfusion system allows the precise targeting of one or a few cells without affecting the surrounding environment (Ainla et al., 2010; Ainla et al., 2012; Wright et al., 2018). A more detailed description of the stimulation and washout steps is described in the method section.

Stimulation of cells expressing the CXCR4-FlAsH228-CFP sensor with CXCL12 induced a rapid increase in the FlAsH signal and a simultaneous decrease in the CFP signal, which led to an increase in the FRET ratio by 2-5% (2.8 ± 0.7 %; mean ± SD) (**Figures 2A-B and S1G**). Using this sensor, activation of CXCR4 occurred with a time constant τ = 590 (440-710) ms (median and IQR) in response to CXCL12 (**Figure 2C-D**). Similar responses were observed when the CXCR4-FlAsH226-CFP and CXCR4-FlAsH229-CFP sensors were used to resolve the kinetics of receptor activation (τ = 600 (360-820) ms and τ = 530 (400-660) ms, respectively; **Figure S1D**). However, the amplitudes of the ligand-induced FRET signals with these two sensors were smaller than with CXCR4-FlAsH228-CFP (2.1 ± 0.6 % for CXCR4-FlAsH226-CFP and 1.7 ± 0.6 % for CXCR4-FlAsH229-CFP; **Figure S1E-G**). After stimulation, rapid superfusion of the cells with buffer removed the ligand and the FRET signal returned to baseline, allowing the off-kinetics of the receptor to be determined. Deactivation of CXCR4 after CXCL12 stimulation occurred with τ = 20.7 (11.6-27.1) s (**Figure 2E**). In summary, these sensors faithfully monitor the ligand-induced structural rearrangements within the TM domain that reflect the activation of the receptor, and have shown that the CXCL12-induced activation of CXCR4 is slower in comparison to other class A GPCRs and more similar to the activation of the class B PTHR.

**CXCR4 and $G_i$ proteins remain within FRET distance in the absence of agonist.**

Molecular Pharmacology Fast Forward. Published on May 30, 2020 as DOI: 10.1124/mol.119.118448
This article has not been copyedited and formatted. The final version may differ from this version.



Generally, activation of a GPCR results in the recruitment of G proteins to the agonist-bound receptor. To determine the speed of coupling, we employed the constructs CXCR4-YFP and $G\gamma_2$-CFP, co-expressed with the $G\alpha_{i1}$ and $G\beta_1$ subunits for proper stoichiometry and localization of the G proteins to the plasma membrane (**Figure 3A**). Surprisingly and in contrast to what has been described for most GPCRs (Hein et al., 2005; Hein et al., 2006; Ferrandon et al., 2009; Hoffmann et al., 2012), stimulation of CXCR4 with CXCL12 (30 μM) resulted in a decrease in the FRET signal with an amplitude of 3.3 ± 1.0 % (**Figure 3C**). This rearrangement occurred at a speed of $\tau$ = 960 (870-980) ms (**Figure 3E**). To further investigate this effect, we examined the interaction of CXCR4-YFP with the G protein CFP-labeled at $G\alpha_{i1}$ ($G\alpha_{i1}$-CFP) (**Figure 3B**). Again, a decrease in the agonist-dependent FRET signal was detected upon receptor activation with an amplitude of 2.7 ± 0.9 % (**Figure 3D**) and at a speed of $\tau$ = 1030 (750-1320) ms (**Figure 3E**).

Whether receptors are preassembled with G proteins or only associate upon agonist exposure is still a matter of debate and, so far, it seems to be dependent on the specific receptor/G protein pair (Hein and Bünemann, 2009; Andressen et al., 2018). To further study a potential interaction of CXCR4 with the $G_i$ protein in the absence of agonist, we performed acceptor photobleaching experiments in cells expressing CXCR4-YFP, $G\gamma_2$-CFP, $G\beta_1$, and $G\alpha_{i1}$ (**Figure 4A**). In parallel, the YFP-labeled $\alpha_{2A}$-AR was tested under the same conditions. CFP and YFP emission intensities were measured prior to and after photobleaching the YFP, and the changes detected in the CFP fluorescence ($F_{CFP}$) were quantified. After photobleaching, no significant increase in $F_{CFP}$ was detected with the $\alpha_{2A}$-AR-YFP ($\Delta F_{CFP}$ = 0.4 (-1.0-1.1) %; median and IQR; **Figure 4B-C**), in agreement with published data (Hein et al., 2005). In contrast, a significant increase in $F_{CFP}$ was detected with CXCR4-YFP ($\Delta F_{CFP}$ = 2.0 (1.0-3.1) %; **Figure 4B and 4D**), indicating the existence of basal energy transfer prior to the photobleaching process. When such cells were treated with 10 μM of the small molecule IT1t (antagonist), no significant change in $F_{CFP}$ upon YFP photobleaching was detected ($\Delta F_{CFP}$ = 0.4 (-0.4-1.2) %; **Figure 4B and 4E**). These findings suggest that while there is no specific interaction between $\alpha_{2A}$-AR and the $G_i$ proteins in the absence of agonist under these experimental conditions, CXCR4 resides within FRET distance of the $G_i$ protein, which might reflect a potential interaction between

Molecular Pharmacology Fast Forward. Published on May 30, 2020 as DOI: 10.1124/mol.119.118448
This article has not been copyedited and formatted. The final version may differ from this version.



these two partners in the absence of agonist. Such behavior is consistent with other studies that suggest that CXCR4 exhibits some degree of basal receptor activity (Mishra et al., 2016; Mona et al., 2016).

**CXCR4 induces prolonged $G_i$ protein activation in response to CXCL12.**

In order to investigate the kinetics of $G_i$ protein activation, we used FRET-based sensors for $G_{i1}$, $G_{i2}$, and $G_{i3}$ (van Unen et al., 2016). These sensors provide a real-time read-out for G protein activation by the loss of FRET between the Gγ- and Gα-labeled subunits in response to agonist stimulation of the receptor (**Figure 5A**). HEK293 cells were co-transfected with CXCR4 or $\alpha_{2A}$-AR and one of the three G protein sensors. Then, single cells were stimulated with the appropriate ligand, either CXCL12 (30 μM) or norepinephrine (100 μM), using the Biopen®. We detected activation of all three G protein subtypes via both receptors in response to their respective agonists, with no significant differences among the G protein subtypes. Upon stimulation, an immediate decrease in the FRET ratio was observed in every case (**Figures 5B-C and S3A-D**). Interestingly, the kinetic profiles of G protein activation via the two receptors were remarkably different. For CXCR4, G protein activation occurred with $\tau \approx 4$ s, while for $\alpha_{2A}$-AR, G protein activation occurred with $\tau \approx 650$ ms (**Figure 5D**), which is almost an order of magnitude faster and in agreement with published data (Hein et al., 2005; Van Unen et al., 2016). After ligand exposure, cells were continuously washed with buffer in order to remove the ligands. In the case of the $\alpha_{2A}$-AR, washing resulted in the FRET signal returning rapidly to baseline, which suggests that the G proteins rapidly adopt once again the inactive conformation upon removal of the ligand. However, CXCL12 induced a prolonged $G_i$ activation via CXCR4, reflected by slower G protein off-kinetics that could not be resolved in the time frame of the experiment (**Figure 5B-C, lower panels; Figure S3A-D**). These observations suggest different G protein activation by these two receptors, even though they both belong to class A GPCRs.

Further experiments were performed in a 96-well plate FRET reader in order to test the effects of CXCL12-induced CXCR4 activation on G proteins. We observed a concentration-dependent activation of $G_{i1}$, $G_{i2}$, and $G_{i3}$ in cells expressing CXCR4 (**Figure 5E, gray lines**). The $EC_{50}$ values obtained for CXCL12 were 6.7 [2.9-15.4] nM for $G_{i1}$ activation, 9.9 [4.8-20.2] nM for $G_{i2}$ activation, and 18.6 [8.4-40.9] nM for $G_{i3}$ activation. Therefore, the isoforms $G_{i1}$ and $G_{i2}$ were activated with

Molecular Pharmacology Fast Forward. Published on May 30, 2020 as DOI: 10.1124/mol.119.118448
This article has not been copyedited and formatted. The final version may differ from this version.



significantly higher potency than $G_{i3}$, which is in accordance with published data (Kleemann et al., 2008). The $EC_{50}$ values obtained are also in good agreement with the potency of CXCL12 at CXCR4 described in other systems (Gupta et al., 2001; Rosenkilde et al., 2004; Kleemann et al., 2008; Levoye et al., 2009). No G protein activation was detected in cells expressing the G protein sensors but not CXCR4 (**Figure 5E, black data points;** controls for $G_{i2}$ and $G_{i3}$ not shown). Although the CXCL12/CXCR4 axis has also been shown to activate $G_q$ proteins in some contexts (Soede et al., 2001; Shi et al., 2007), we did not detect activation of $G_q$ using a FRET-based $G_q$ sensor (**Figure 5E, brown data points;** Adjobo-Hermans et al., 2011).

Since our data suggest a potential interaction between CXCR4 and G proteins in the absence of agonist, we next analyzed the effects of IT1t *versus* those of CXCL12 on the $G_{i2}$ FRET sensor in CXCR4-expressing cells. FRET was analyzed under different conditions: buffer treatment, 100 µM IT1t treatment, or 100 nM CXCL12 treatment. We observed that IT1t caused a significantly higher FRET, and CXCL12 a significantly lower FRET compared to buffer (**Figure 5F**). These data support the notion that CXCR4 activates G proteins in the absence of agonist, i.e. that it exhibits some degree of basal receptor activity, which can be blocked by IT1t, thus suggesting that this molecule would act as inverse agonist on CXCR4.

**CXCR4 homodimer rearrangement kinetically precedes G protein activation.**

Despite the fact that GPCR monomers have been demonstrated to be functional units (Whorton et al., 2007), increasing evidence has emerged for a functional role of dimers and higher-oligomeric structures (Milligan et al., 2019). Therefore, we next investigated the kinetics of the rearrangement that occurs between CXCR4 protomers upon binding of CXCL12. To do so, HEK293 cells were transfected with CXCR4-CFP and CXCR4-YFP and stimulated with the agonist CXCL12, again using the Biopen® (**Figure 6A**).

Upon stimulation of single cells with CXCL12 (30 µM), a large increase in the FRET signal was detected with an amplitude of 7.5 ± 2.8 %, which suggests an approximation of the two fluorophores in the active state of the receptor (**Figure 6B**). Interestingly, this rearrangement occurred at a speed of

Molecular Pharmacology Fast Forward. Published on May 30, 2020 as DOI: 10.1124/mol.119.118448
This article has not been copyedited and formatted. The final version may differ from this version.



τ = 1660 (1370-2010) ms (**Figure 6C**), which indicates that this movement is achieved faster than the activation of the G proteins. Upon wash-out of the ligand with buffer, the signal returned to baseline, which allowed the determination of the off-kinetics of this process to be τ = 34.1 (21.3-36.1) s (**Figure 6D**). Altogether, these data suggest that changes in CXCR4 homodimer occur slower than activation of a CXCR4 protomer. In contrast to our observations for CXCR4, several reports demonstrated that for the class C mGluR1, inter-subunit rearrangements between protomers precedes intra-subunit rearrangements (Hlavackova et al., 2012; Grushevskyi et al., 2019). This distinct behavior might be related to the different nature of the receptor dimers and might be a characteristic activation feature of class C GPCRs, for which dimerization is obligatory for function (Kniazeff et al., 2011; Zhang et al., 2014).

**MIF induces distinct structural rearrangements in CXCR4 and does not activate $G_i$ proteins.**

MIF has been recently described to be able to bind and signal via CXCR4 as a partial agonist (Rajasekaran et al., 2016). Therefore, the settings that have been earlier established in this work to investigate the CXCL12-induced activation of CXCR4 were employed to investigate each step of the transduction pathway of this receptor in response to MIF. During the measurements, single cells expressing the construct(s) of interest were stimulated with 100 μM MIF, followed by a short wash-out with buffer and subsequent stimulation with 30 μM CXCL12.

First, receptor activation was investigated in cells transfected with the CXCR4-FlAsH228-CFP sensor and FlAsH-labeled prior to the measurement. In contrast to CXCL12, which produced an increase in the FRET signal, MIF binding to the sensor led to a decrease in the FRET ratio at a speed of τ = 270 (250-440) ms (**Figure 7A-B**). This suggests different conformational changes in CXCR4 by these two ligands. Washing of the cells with buffer after MIF stimulation rapidly returned the FRET signal to baseline, indicating that MIF can be easily removed from the receptor and suggesting a low ligand affinity. Subsequent stimulation with CXCL12 produced a response that was undistinguishable from the response observed when cells were directly stimulated with CXCL12, indicating that this response is not affected by the prior stimulation of the cells with MIF (**Figure S4A**). Second, the interaction of CXCR4 with the $G_i$ protein was examined in cells transfected with CXCR4-YFP and the G protein

Molecular Pharmacology Fast Forward. Published on May 30, 2020 as DOI: 10.1124/mol.119.118448
This article has not been copyedited and formatted. The final version may differ from this version.



CFP-labeled at the $G\gamma_2$ subunit. Upon stimulation with MIF, an increase in the FRET signal was observed with $\tau$ = 380 (300-560) ms (**Figure 7C-D**). Thus, again, MIF produced a response that is opposite to that of CXCL12, suggesting that the rearrangement of the $G_i$ protein with CXCR4 is different when the receptor is bound to MIF and CXCL12, and further supports the idea that the receptor adopts distinct conformations when bound to these two ligands. Upon washing of the cells with buffer, the FRET signal rapidly returned to baseline and the cells could be subsequently stimulated with CXCL12, inducing a similar response to when cells are directly stimulated with this ligand (**Figure S4B**). Third, we investigated the movement between CXCR4 protomers upon MIF binding in cells transfected with CXCR4-CFP and CXCR4-YFP. We observed a MIF-induced decrease in the FRET signal that occurred at a speed of $\tau$ = 870 (580-930) ms (**Figure 7E-F**). Again, the signal induced by MIF moved in the opposite direction, indicating once again different conformational changes in the receptor induced by these two ligands. The response induced by CXCL12 was also not affected by prior stimulation of the cells with MIF (**Figure S4C**). Fourth, cells transfected with CXCR4 and the $G_{i2}$ sensor were employed to investigate receptor-mediated G protein activation. Surprisingly, stimulation of the cells with MIF did not result in a change in FRET in the G protein sensor (**Figure 7G**), indicating a lack of CXCR4-mediated G protein activation in response to this ligand. As a positive control, subsequent stimulation of the same cells with CXCL12 led to the activation of the G protein. A summary of the kinetics of CXCR4 activation and signaling in response to MIF in comparison to CXCL12 is shown in **Figure 7H.**

Molecular Pharmacology Fast Forward. Published on May 30, 2020 as DOI: 10.1124/mol.119.118448
This article has not been copyedited and formatted. The final version may differ from this version.



**Discussion**

The temporal resolution of individual biochemical steps that comprise a signaling cascade is important to understand cellular signaling. In this study, we report the kinetic and dynamic properties of early activation events in the CXCR4 transduction pathway in response to CXCL12 and MIF. Based on known movements of the TM domains that occur in GPCRs upon activation (Latorraca et al., 2017), we developed FRET-based sensors that are able to faithfully report the ligand-induced conformational changes in CXCR4. These constructs localize to the plasma membrane and preserve the ability to activate G proteins (**Figure 1**), representing the first FRET sensors developed in the field of chemokine receptors.

The CXCR4 FRET sensors exhibited activation kinetics of $\tau \approx 600$ ms in response to binding of the peptide agonist CXCL12 (**Figure 2**). This is considerably slower than other class A receptors in response to small molecules, which exhibit activation time constants in the range of 2-50 ms (Vilardaga et al., 2003; Hoffmann et al., 2005; Rochais et al., 2007; Reiner et al., 2010; Ziegler et al., 2011; Grushevskyi et al., 2019). Interestingly, CXCL12-induced activation of CXCR4 occurred in the same time range as the activation kinetics determined for the class B PTHR in response to the peptide PTH(1-34) ($\tau \approx 1$ s; Vilardaga et al., 2003). These differences in the activation kinetics might depend on intrinsic properties of the receptors, the type of ligand and its binding-mode. In this case, the binding of chemokines to their chemokine receptors proceeds via a complex mechanism that involves the formation of an extensive protein-protein interface with multiple recognition sites throughout the receptor (Wu et al., 2010; Kleist et al., 2016; Gustavsson et al., 2017). Likewise, PTH(1-34) was described to bind in two steps to PTHR (Castro et al., 2005).

The next signaling step we investigated led to the interesting observation of a decrease in the FRET signal between CXCR4-YFP and the CFP-labeled G protein upon CXCL12 stimulation (**Figure 3**). Most receptors tested using this setting reported an increase in the FRET signal upon agonist stimulation, which is interpreted as G protein recruitment by the receptor (Hein et al., 2005; Hein et al., 2006). A recent study comparing the propensity of the two serotonin receptors 5-$HT_4$ and 5-$HT_7$ to associate with G proteins showed that 5-$HT_7$ pre-associates with $G_s$, while 5-$HT_4$ interacts with $G_s$ in

Molecular Pharmacology Fast Forward. Published on May 30, 2020 as DOI: 10.1124/mol.119.118448
This article has not been copyedited and formatted. The final version may differ from this version.



an agonist-dependent manner. Respectively, a decrease and increase in the FRET signals was detected (Andressen et al., 2018). Accordingly, our data might suggest that CXCL12 stimulation of CXCR4 does not lead to recruitment of the G protein but rather to a rearrangement or dissociation of a preformed complex.

The spontaneous ligand-independent transition of GPCRs between inactive and active conformations is called basal or constitutive activity, and is a common property of wt GPCRs, but can also be a result of receptor mutations, which can cause a variety of diseases (Seifert and Wenzel-Seifert, 2002). Our results suggest a significant degree of basal activity for CXCR4. Photobleaching experiments in cells expressing CXCR4-YFP and CFP-labeled $G_{i1}$ protein showed a ligand-independent energy transfer between these two proteins (**Figure 4**). Although the nature of their interaction is unknown, these data suggest close proximity or potential interaction between CXCR4 and the $G_i$ protein prior to agonist stimulation. This hypothesis is further supported by the basal activation of $G_i$ proteins observed in the presence of CXCR4, which was abolished by addition of IT1t, hence indicating inverse agonist properties for this compound (**Figure 4 and 5F**). Considering that an estimated 85% of antagonists turn out to be inverse agonists when tested in contexts in which receptors exhibit constitutive activity (Kenakin, 2004), it is not surprising that IT1t, considered a CXCR4 antagonist until now, exhibits inverse agonist properties in our assays. Although our findings indicate that CXCR4 exhibits constitutive activity (at least in regard to G protein signaling), stimulation of the cells with CXCL12 further activated G proteins, thus indicating that this activity was not saturated. The existence of basal CXCR4 activity is in agreement with observations in previous studies (Mishra et al., 2016; Mona et al., 2016). Since overexpression of CXCR4 has been widely reported for a large number of cancers and other pathologies (Müller et al., 2001; Balkwill, 2004; Darash-Yahana et al., 2004; Chatterjee et al., 2014b; Zhao et al., 2015), the degree of spontaneous activity might reach a significant level in these contexts and become therapeutically relevant. On the basis of our observations, the degree of basal activity of CXCR4 should be validated in such pathophysiological systems and in vivo. An in depth understanding of the biology of CXCR4 in this respect should assist in the design of improved CXCR4-targeting drugs.

Molecular Pharmacology Fast Forward. Published on May 30, 2020 as DOI: 10.1124/mol.119.118448
This article has not been copyedited and formatted. The final version may differ from this version.



When measuring G protein activation, we made an intriging observation related to the G protein off-kinetics. Even after persistent wash-out of CXCL12 from the receptor, CXCR4-mediated G protein activation remained for a long time (**Figure 5B**), while this was not the case for the norepinephrine/$\alpha_{2A}$-AR axis (**Figure 5C**) or other ligand/receptor pairs tested using these same G protein sensors (van Unen et al., 2016; Oehler et al., 2017; Grundmann et al., 2018). The nature of this observation is currently unknown to us, but several factors might play a role in this process. A possible explanation might be related to ligand residence time that might contribute to prolonged signaling (Hoffmann et al., 2015; Hothersall et al., 2016). Compared to norepinephrine and $\alpha_{2A}$-AR, CXCL12 remains bound to CXCR4 for a significantly longer time period. This assumption is based on our observed slower CXCR4 off-kinetics upon CXCL12 stimulation and wash-out with buffer, which was roughly ≈21 seconds (**Figure 2E**), hence approximately 10 times slower than the $\alpha_{2A}$-AR sensor (Hein et al., 2005). However, this deactivation of the CXCR4 receptor was still much faster than the G protein deactivation. Alternatively, the different receptors might induce distinct active conformations of the G protein, which would display different lifetimes and GTPase activities (Furness et al., 2016). To mechanistically explain these differences in G protein off-kinetics, further research is required.

Our study provides insights into the distinct mechanisms by which MIF and CXCL12 regulate the activity of CXCR4 and presents evidence for their different pharmacological properties. Our data indicate that binding of CXCL12 and MIF induce distinct structural rearrangements in CXCR4, which can be distinguished dynamically and kinetically at each step of the signaling cascade (**Figure 7**). This suggests different binding modes of these two ligands to the same receptor, as proposed by other studies (Rajasekaran et al., 2016; Lacy et al., 2018). The extensive interaction interface between CXCL12 and CXCR4 involves interactions between the core of the ligand and the receptor N-terminus, as well as the ligand N-terminus with the receptor TM cavity (Qin et al., 2015). In contrast, MIF binds to the N-terminal region of CXCR4 at different residues than CXCL12 and not within the TM cavity (Rajasekaran et al., 2016). Their different binding modes are also supported by the incomplete displacement of CXCL12 from CXCR4 by MIF (**Figure S5**; Bernhagen et al., 2007). Furthermore, and in line with our distinct FRET signals (MIF opposite to CXCL12), but in contrast to

Molecular Pharmacology Fast Forward. Published on May 30, 2020 as DOI: 10.1124/mol.119.118448
This article has not been copyedited and formatted. The final version may differ from this version.



other studies, we did not detect $G_i$ protein activation via CXCR4 in response to MIF (**Figure 7G**). While our observations would suggest inverse agonist properties for MIF, functional data in other studies show that MIF acts as a CXCR4 allosteric partial agonist and mediates at least some of its functions via $G_i$ proteins (Bernhagen et al., 2007; Klasen et al., 2014; Rajasekaran et al., 2016). A possible explanation for these distinct observations could be the cellular context. While MIF can bind to CXCR4 alone, its binding and function appears to be facilitated by the presence of the single-pass membrane-receptor CD74 (Cluster of Differentiation 74), which together with CXCR4 form a functional high-affinity heteromeric complex for MIF (Bernhagen et al., 2007; Schwartz et al., 2009; Klasen et al., 2014). HEK293 cells lack endogenous expression of CD74 (Schwartz et al., 2009) and, in our experiments, MIF was rapidly washed away from the receptor upon addition of buffer (**Figure 7A, C and E**). The presence of CXCR4/CD74 complexes, might be crucial in determining MIF signaling. For example, in platelets, which lack CD74, MIF could bind to CXCR4 but did not lead to ERK phosphorylation, while MIF-induced ERK phosphorylation was detected in monocytes, which express both receptors (Chatterjee et al., 2014a).

In summary, we provide kinetic data from ensemble measurements for the early signaling steps of the human chemokine receptor CXCR4. Upon CXCL12 engagement, structural rearrangements within the TM domain ($\tau \approx 600$ms) are kinetically followed by rearrangements between CXCR4 and the G protein in the intracellular side that occur at a speed of $\tau \approx 1$s. Furthermore, a structural rearrangement between CXCR4 protomers occurs with $\tau \approx 1.7$s, while G protein activation by CXCR4 finally occurs with $\tau \approx 4$s. These kinetic events are summarized in **Figure 8**. It is tempting to speculate that the rearrangement between protomers precedes G protein activation and to suggest that conformational changes in CXCR4 homodimers, when present, play a possible role in the signaling activation course of this receptor as depicted in model B. However, we need to emphasize that mechanistic interpretation needs to be based on measuring microscopic rate constants and hence model A, where dimer rearrangement offers an alternative pathway, is also compatible with our dataset.

Molecular Pharmacology Fast Forward. Published on May 30, 2020 as DOI: 10.1124/mol.119.118448
This article has not been copyedited and formatted. The final version may differ from this version.



**Acknowledgements**

We thank all colleagues from ONCORNET for helpful scientific discussions.

Molecular Pharmacology Fast Forward. Published on May 30, 2020 as DOI: 10.1124/mol.119.118448
This article has not been copyedited and formatted. The final version may differ from this version.



**Authorship Contributions**

Participated in research design: Perpiñá-Viciano, Zarca, Kilpatrick, Hoffmann

Conducted experiments: Perpiñá-Viciano, Zarca, Kilpatrick, Caspar

Performed data analysis: Perpiñá-Viciano, Zarca, Kilpatrick, Caspar

Wrote or contributed to the writing of the manuscript: Perpiñá-Viciano, Işbilir, Kilpatrick, Hoffmann, Lohse, Smit, Hill

Molecular Pharmacology Fast Forward. Published on May 30, 2020 as DOI: 10.1124/mol.119.118448
This article has not been copyedited and formatted. The final version may differ from this version.



**References**

Adjobo-Hermans MJ, Goedhart J, van Weeren L, Nijmeijer S, Manders EM, Offermanns S, and Gadella TWJ (2011) Real-time visualization of heterotrimeric G protein Gq activation in living cells. *BMC Biol* **9:** 32.

Adlere I, Caspar B, Arimont M, Dekkers S, Visser K, Stuijt J, de Graaf C, Stocks M, Kellam B, Briddon S, Wijtmans M, de Esch I, Hill S, and Leurs R (2019) Modulators of CXCR4 and CXCR7/ACKR3 function. *Mol Pharmacol.* **96**:737-752

Ainla A, Jansson ET, Stepanyants N, Orwar O, and Jesorka A (2010) A microfluidic pipette for single-cell pharmacology. *Anal Chem* **82:** 4529-4536.

Ainla A, Jeffries GD, Brune R, Orwar O, and Jesorka A (2012) A multifunctional pipette. *Lab Chip* **12:** 1255-1261.

Alsayed Y, Ngo H, Runnels J, Leleu X, Singha UK, Pitsillides CM, Spencer JA, Kimlinger T, Ghobrial JM, Jia X, Lu G, Timm M, Kumar A, Côté D, Veilleux I, Hedin KE, Roodman GD, Witzig TE, Kung AL, Hideshima T, Anderson KC, Lin CP, and Ghobrial IM (2007) Mechanisms of regulation of CXCR4/SDF-1 (CXCL12)-dependent migration and homing in multiple myeloma. *Blood* **109:** 2708-2717.

Altenbach C, Kusnetzow AK, Ernst OP, Hofmann KP, and Hubbell WL (2008) High-resolution distance mapping in rhodopsin reveals the pattern of helix movement due to activation. *PNAS* **105:** 7439-7444.

Andressen KW, Ulsund AH, Krobert KA, Lohse MJ, Bünemann M, and Levy FO (2018) Related GPCRs couple differently to Gs: preassociation between G protein and 5-HT7 serotonin receptor reveals movement of Gαs upon receptor activation. *FASEB J* **32:** 1059-1069.

Balkwill F (2004) The significance of cancer cell expression of the chemokine receptor CXCR4. *Semin Cancer Biol* **14:** 171-179.

Molecular Pharmacology Fast Forward. Published on May 30, 2020 as DOI: 10.1124/mol.119.118448
This article has not been copyedited and formatted. The final version may differ from this version.



Bernhagen J, Krohn R, Lue H, Gregory JL, Zernecke A, Koenen RR, Dewor M, Georgiev I, Schober A, Leng L, Kooistra T, Fingerle-Rowson G, Ghezzi P, Kleemann R, McColl SR, Bucala R, Hickey MJ, and Weber C (2007) MIF is a non-cognate ligand of CXC chemokine receptors in inflammatory and atherogenic cell recruitment. *Nat Med* **13:** 587-596.

Bobkov V, Arimont M, Zarca A, De Groof T, van der Woning B, de Haard H, and Smit MJ (2019) Antibodies targeting chemokine receptors CXCR4 and ACKR3. *Mol Pharmacol* **96**:753-764.

Bünemann M, Frank M, and Lohse MJ (2003) Gi protein activation in intact cells involves subunit rearrangement rather than dissociation. *PNAS* **100:** 16077-16082.

Castro M, Nikolaev VO, Palm D, Lohse MJ, and Vilardaga JP (2005) Turn-on switch in parathyroid hormone receptor by a two-step parathyroid hormone binding mechanism. *Proc Natl Acad Sci USA* **102:** 16084-16089.

Chatterjee M, Borst O, Walker B, Fotinos A, Vogel S, Seizer P, Mack A, Alampour-Rajabi S, Rath D, Geisler T, Lang F, Langer HF, Bernhagen J, and Gawaz M (2014a) Macrophage migration inhibitory factor limits activation-induced apoptosis of platelets via CXCR7-dependent Akt signaling. *Circ Res* **115:** 939-49.

Chatterjee S, Behnam Azad B, and Nimmagadda S (2014b) The intricate role of CXCR4 in cancer. *Adv Cancer Res* **124:** 31-82.

Chung KY (2013) Structural Aspects of GPCR-G Protein Coupling. *Toxicol Res* **29:** 149-155.

Darash-Yahana M, Pikarsky E, Abramovitch R, Zeira E, Pal B, Karplus R, Beider K, Avniel S, Kasem S, Galun E, and Peled A (2004) Role of high expression levels of CXCR4 in tumor growth, vascularization, and metastasis. *FASEB J* **18:** 1240-2.

Ferrandon S, Feinstein TN, Castro M, Wang B, Bouley R, Potts JT, Gardella TJ, and Vilardaga JP (2009) Sustained cyclic AMP production by parathyroid hormone receptor endocytosis. *Nat Chem Biol* **5:** 734-742.

Molecular Pharmacology Fast Forward. Published on May 30, 2020 as DOI: 10.1124/mol.119.118448
This article has not been copyedited and formatted. The final version may differ from this version.



Furness SGB, Liang YL, Nowell CJ, Halls ML, Wookey PJ, Dal Maso E, Inoue A, Christopoulos A, Wootten D, and Sexton PM (2016) Ligand-Dependent Modulation of G Protein Conformation Alters Drug Efficacy. *Cell* **167:** 739-749.

Grundmann M, Merten N, Malfacini D, Inoue A, Preis P, Simon K, Rüttiger N, Ziegler N, Benkel T, Schmitt NK, Ishida S, Müller I, Reher R, Kawakami K, Inoue A, Rick U, Kühl T, Imhof D, Aoki J, König GM, Hoffmann C, Gomeza J, Wess J, and Kostenis E (2018) Lack of beta-arrestin signaling in the absence of active G proteins. *Nat Commun* **9:** 341.

Grushevskyi EO, Kukaj T, Schmauder R, Bock A, Zabel U, Schwabe T, Benndorf K, and Lohse MJ (2019) Stepwise activation of a class C GPCR begins with millisecond dimer rearrangement. *Proc Natl Acad Sci USA* **116:** 10150-10155.

Guo F, Wang Y, Liu J, Mok SC, Xue F, and Zhang W (2016) CXCL12/CXCR4: a symbiotic bridge linking cancer cells and their stromal neighbors in oncogenic communication networks. *Oncogene* **35:** 816-26.

Gupta SK, Pillarisetti K, Thomas RA, and Aiyar N (2001) Pharmacological evidence for complex and multiple site interaction of CXCR4 with SDF-1alpha: implications for development of selective CXCR4 antagonists. *Immunol Lett* **78:** 29-34.

Gustavsson M, Wang L, van Gils N, Stephens BS, Zhang P, Schall TJ, Yang S, Abagyan R, Chance MR, Kufareva, I, and Handel TM (2017) Structural basis of ligand interaction with atypical chemokine receptor 3. *Nat Commun* **8:** 14135.

Hein P, Frank M, Hoffmann C, Lohse MJ, and Bünemann M (2005) Dynamics of receptor/G protein coupling in living cells. *EMBO J* **24:** 4106-4114.

Hein P, Rochais F, Hoffmann C, Dorsch S, Nikolaev VO, Engelhardt S, Berlot CH, Lohse MJ, and Bünemann M (2006) Gs activation is time-limiting in initiating receptor-mediated signaling. *J Biol Chem* **281:** 33345-51.

Molecular Pharmacology Fast Forward. Published on May 30, 2020 as DOI: 10.1124/mol.119.118448
This article has not been copyedited and formatted. The final version may differ from this version.



Hein P and Bünemann M (2009) Coupling mode of receptors and G proteins. *Naunyn Schmiedebergs Arch Pharmacol* **379:** 435-443.

Heuninck J, Perpiñá Viciano C, Işbilir A, Caspar B, Capoferri D, Briddon SJ, Durroux T, Hill SJ, Lohse MJ, Milligan G, Pin JP, and Hoffmann C (2019) Context-dependent signalling of CXC chemokine receptor 4 (CXCR4) and atypical chemokine receptor 3 (ACKR3). *Mol Pharmacol* **96**:778-793.

Hilger D, Masureel M, and Kobilka BK (2018) Structure and dynamics of GPCR signaling complexes. *Nat Struct Mol Biol* **25:** 4-12.

Hlavackova V, Goudet C, Kniazeff J, Zikova A, Maurel D, Vol C, Trojanova J, Prézeau L, Pin JP, and Blahos J (2005) Evidence for a single heptahelical domain being turned on upon activation of a dimeric GPCR. *EMBO J* **24:** 499-509.

Hlavackova V, Zabel U, Frankova D, Bätz J, Hoffmann C, Prezeau L, Pin JP, Blahos J, and Lohse MJ (2012) Sequential inter- and intrasubunit rearrangements during activation of dimeric metabotropic glutamate receptor 1. *Sci Signal* **5:** ra59.

Hoffmann C, Gaietta G, Bünemann M, Adams SR, Oberdorff-Maass S, Behr B, Vilardaga JP, Tsien RY, Ellisman MH, and Lohse MJ (2005) A FlAsH-based FRET approach to determine G protein-coupled receptor activation in living cells. *Nat Methods* **2:** 171-176.

Hoffmann C, Gaietta G, Zürn A, Adams SR, Terrillon S, Ellisman MH, Tsien RY, and Lohse MJ (2010) Fluorescent labeling of tetracysteine-tagged proteins in intact cells. *Nat Protoc* **5:** 1666-1677.

Hoffmann C, Nuber S, Zabel U, Ziegler N, Winkler C, Hein P, Berlot CH, Bünemann M, and Lohse MJ (2012) Comparison of the activation kinetics of the m3 acetylcholine receptor and a constitutively active mutant receptor in living cells. *Mol Pharmacol* **82:** 236-245.

Molecular Pharmacology Fast Forward. Published on May 30, 2020 as DOI: 10.1124/mol.119.118448
This article has not been copyedited and formatted. The final version may differ from this version.



Hoffmann C, Castro M, Rinken A, Leurs R, Hill SJ and Vischer HF (2015) Ligand Residence Time at G-protein-Coupled Receptors-Why We Should Take Our Time To Study It. *Mol Pharmacol* **88**:552-560.

Hothersall JD, Brown AJ, Dale I, and Rawlins P (2016) Can residence time offer a useful strategy to target agonist drugs for sustained GPCR responses?. *Drug Discov Today* **21:** 90-96.

Hu J, Wang Y, Zhang X, Lloyd JR, Li J, Karpiak J, Costanzi S, and Wess J (2010) Structural basis of G protein-coupled receptor/G protein interactions. *Nat Chem Biol* **6:** 541-548.

Jost CA, Reither G, Hoffmann C, and Schultz C (2008) Contribution of fluorophores to protein kinase C FRET probe performance. *Chembiochem* ***9:*** 1379-1384.

Kenakin T (2004) Efficacy as a vector: the relative prevalence and paucity of inverse agonism. *Mol Pharmacol* **65:** 2-11.

Klasen C, Ohl K, Sternkopf M, Shachar I, Schmitz C, Heussen N, Hobeika E, Levit-Zerdoun E, Tenbrock K, Reth M, Bernhagen J and El Bounkari O (2014) MIF promotes B cell chemotaxis through the receptors CXCR4 and CD74 and ZAP-70 signaling. *J Immunol* **192**:5273-5284.

Kleemann P, Papa D, Vigil-Cruz S, and Seifert R (2008) Functional reconstitution of the human chemokine receptor CXCR4 with G(i)/G(o)-proteins in Sf9 insect cells. *Naunyn-Schmiedeberg's Arch Pharmacol* **378:** 261-74.

Kleist AB, Getschman AE, Ziarek JJ, Nevins AM, Gauthier PA, Chevigné A, Szpakowska M, and Volkman BF (2016) New paradigms in chemokine receptor signal transduction: Moving beyond the two-site model. *Biochem Pharmacol* **114:** 53-68.

Kniazeff J, Saintot PP, Goudet C, Liu J, Charnet A, Guillon G, and Pin JP (2004) Locking the dimeric GABA(B) G-protein-coupled receptor in its active state. *J Neurosci* **24:** 370-7.

Molecular Pharmacology Fast Forward. Published on May 30, 2020 as DOI: 10.1124/mol.119.118448
This article has not been copyedited and formatted. The final version may differ from this version.



Kniazeff J, Prézeau L, Rondard P, Pin JP, and Goudet C (2011) Dimers and beyond: The functional puzzles of class C GPCRs. *Pharmacol Ther* **130:** 9-25.

Lacy M, Kontos C, Brandhofer M, Hille K, Gröning S, Sinitski D, Bourilhon P, Rosenberg E, Krammer C, Thavayogarajah T, Pantouris G, Bakou M, Weber C, Lolis E, Bernhagen J, and Kapurniotu A (2018) Identification of an Arg-Leu-Arg tripeptide that contributes to the binding interface between the cytokine MIF and the chemokine receptor CXCR4. *Sci Rep* **8:** 5171.

Latorraca NR, Venkatakrishnan AJ, and Dror RO (2017) GPCR Dynamics: Structures in Motion. *Chem Rev* **117:** 139-155.

Levoye A, Balabanian K, Baleux F, Bachelerie F, and Lagane B (2009) CXCR7 heterodimerizes with CXCR4 and regulates CXCL12-mediated G protein signaling. *Blood* **113:** 6085-6093.

Lohse MJ, Nuber S, and Hoffmann C (2012) Fluorescence/Bioluminescence Resonance Energy Transfer Techniques to Study G-Protein-Coupled Receptor Activation and Signaling. *Pharmacol Rev* **64:** 299-336.

Lohse MJ, Maiellaro I, and Calebiro D (2014) Kinetics and mechanism of G protein-coupled receptor activation. *Curr Opin Cell Biol* **27:** 87-93.

Messerer R, Kauk M, Volpato D, Alonso Cañizal MC, Klöckner J, Zabel U, Nuber S, Hoffmann C, and Holzgrabe U (2017) FRET Studies of Quinolone-Based Bitopic Ligands and Their Structural Analogues at the Muscarinic M1 Receptor. *ACS Chem Biol* **12:** 833-843.

Milligan G, Ward RJ, and Marsango S (2019) GPCR homo-oligomerization. *Curr Opin Cell Biol* **57:** 40-47.

Mishra RK, Shum AK, Platanias LC, Miller RJ, and Schiltzb GE (2016) Discovery and characterization of novel small-molecule CXCR4 receptor agonists and antagonists. *Sci Rep* **6:** 30155.

Molecular Pharmacology Fast Forward. Published on May 30, 2020 as DOI: 10.1124/mol.119.118448
This article has not been copyedited and formatted. The final version may differ from this version.



Mona CE, Besserer-Offroy E, Cabana J, Leduc R, Lavigne P, Heveker N, Marsault E, and Escher E (2016) Design, synthesis, and biological evaluation of CXCR4 ligands. *Org Biomol Chem* **14:** 10298-10311.

Müller A, Homey B, Soto H, Ge N, Catron D, Buchanan ME, McClanahan T, Murphy E, Yuan W, Wagner SN, Barrera JL, Mohar A, Verástegui E, and Zlotnik A (2001) Involvement of chemokine receptors in breast cancer metastasis. *Nature* **410:** 50-6.

Oehler B, Mohammadi M, Perpiñá Viciano C, Hackel D, Hoffmann C, Brack A, and Rittner HL (2017) Peripheral Interaction of Resolvin D1 and E1 with Opioid Receptor Antagonists for Antinociception in Inflammatory Pain in Rats. *Front Mol Neurosci* **10:** 242.

Qin L, Kufareva I, Holden LG, Wang C, Zheng Y, Zhao C, Fenalti G, Wu H, Han GW, Cherezov V, Abagyan R, Stevens RC, and Handel TM (2015) Crystal structure of the chemokine receptor CXCR4 in complex with a viral chemokine. *Science* **347:** 1117-1122.

Rajasekaran D, Gröning S, Schmitz C, Zierow S, Drucker N, Bakou M, Kohl K, Mertens A, Lue H, Weber C, Xiao A, Luker G, Kapurniotu A, Lolis E, and Bernhagen J (2016) Macrophage Migration Inhibitory Factor-CXCR4 Receptor Interactions: evidence for partial allosteric agonism in comparison with CXCL12 chemokine. *J Biol Chem* **291:** 15881-95.

Reiner S, Ambrosio M, Hoffmann C, and Lohse MJ (2010) Differential signaling of the endogenous agonists at the beta2-adrenergic receptor. *Journal Biol Chem* **285:** 36188-36198.

Rochais F, Vilardaga JP, Nikolaev VO, Bünemann M, Lohse MJ, and Engelhardt S (2007) Real-time optical recording of beta1-adrenergic receptor activation reveals supersensitivity of the Arg389 variant to carvedilol. *J Clin Invest* **117:** 229-235.

Rosenkilde MM, Gerlach LO, Jakobsen JS, Skerlj RT, Bridger GJ, and Schwartz TW (2004) Molecular mechanism of AMD3100 antagonism in the CXCR4 receptor: transfer of binding site to the CXCR3 receptor. *J Biol Chem* **279:** 3033-41.

Molecular Pharmacology Fast Forward. Published on May 30, 2020 as DOI: 10.1124/mol.119.118448
This article has not been copyedited and formatted. The final version may differ from this version.



Schwartz V, Lue H, Kraemer S, Korbiel J, Krohn R, Ohl K, Bucala R, Weber C, and Bernhagen J (2009) A functional heteromeric MIF receptor formed by CD74 and CXCR4. *FEBS Lett* **583:** 2749-57.

Seifert R and Wenzel-Seifert K (2002) Constitutive activity of G-protein-coupled receptors: cause of disease and common property of wild-type receptors. *Naunyn Schmiedebergs Arch Pharmacol* **366:** 381-416.

Shi G, Partida-Sánchez S, Misra RS, Tighe M, Borchers MT, Lee JJ, Simon MI, and Lund FE (2007) Identification of an alternative G{alpha}q-dependent chemokine receptor signal transduction pathway in dendritic cells and granulocytes. *J Exp Med* **204:** 2705-18.

Stoddart LA, Johnstone E, Wheal AJ, Goulding J, Robers MB, Machleidt T, Wood KV, Hill SJ, and Pfleger K (2015) Application of BRET to monitor ligand binding to GPCRs. *Nat methods* **12:** 661-663.

Stumpf AD and Hoffmann C (2016) Optical probes based on G protein-coupled receptors - added work or added value?. *Br J Pharmacol* **173:** 255-266.

Soede RD, Zeelenberg IS, Wijnands YM, Kamp M, and Roos E (2001) Stromal cell-derived factor-1-induced LFA-1 activation during in vivo migration of T cell hybridoma cells requires Gq/11, RhoA, and myosin, as well as Gi and Cdc42. *J Immunol* **166:** 4293-4301.

Tsibris AM and Kuritzkes DR (2007) Chemokine antagonists as therapeutics: focus on HIV-1. *Annu Rev Med* **58:** 445-59.

Van Unen J, Stumpf AD, Schmid B, Reinhard NR, Hordijk PL, Hoffmann C, Gadella Jr TWJ, and Goedhart, J (2016) A New Generation of FRET Sensors for Robust Measurement of $G\alpha_{i1}$, $G\alpha_{i2}$and $G\alpha_{i3}$ Activation Kinetics in Single Cells. *PLoS ONE* **11:** e0146789.

Molecular Pharmacology Fast Forward. Published on May 30, 2020 as DOI: 10.1124/mol.119.118448
This article has not been copyedited and formatted. The final version may differ from this version.



Vilardaga JP, Bünemann M, Krasel C, Castro M, and Lohse MJ (2003) Measurement of the millisecond activation switch of G protein-coupled receptors in living cells. *Nat Biotechnol* **21:** 807-12.

Vilardaga JP, Steinmeyer R, Harms GS, and Lohse MJ (2005) Molecular basis of inverse agonism in a G protein-coupled receptor. *Nat Chem Biol* **1:** 25-28.

Vilardaga JP, Nikolaev VO, Lorenz K, Ferrandon S, Zhuang Z, and Lohse MJ (2008) Conformational cross-talk between $\alpha_{2A}$-adrenergic and μ-opioid receptors controls cell signaling. *Nat Chem Biol* **4:** 126-131.

Watts AO, van Lipzig MM, Jaeger WC, Seeber RM, van Zwam M, Vinet J, van der Lee MM, Siderius M, Zaman GJ, Boddeke HW, Smit MJ, Pfleger KD, Leurs R, and Vischer HF (2013) Identification and profiling of CXCR3-CXCR4 chemokine receptor heteromer complexes. *Br J Pharmacol* **168:** 1662-74.

Whorton MR, Bokoch MP, Rasmussen SG, Huang B, Zare RN, Kobilka B, and Sunahara RK (2007) A monomeric G protein-coupled receptor isolated in a high-density lipoprotein particle efficiently activates its G protein. *Proc Natl Acad Sci USA* **104:** 7682-7687.

Wright SC, Alonso Cañizal MC, Benkel T, Simon K, Le Gouill C, Matricon P, Namkung Y, Lukasheva V, König GM, Laporte SA, Carlsson J, Kostenis E, Bouvier M, Schulte G, and Hoffmann C (2018) FZD5 is a Gαq-coupled receptor that exhibits the functional hallmarks of prototypical GPCRs. *Sci Signal* **11:** eaar5536.

Wu B, Chien EY, Mol CD, Fenalti G, Liu W, Katritch V, Abagyan R, Brooun A, Wells P, Bi FC, Hamel DJ, Kuhn P, Handel TM, Cherezov V, and Stevens RC (2010) Structures of the CXCR4 chemokine GPCR with small-molecule and cyclic peptide antagonists. *Science* **330:** 1066-71.

Molecular Pharmacology Fast Forward. Published on May 30, 2020 as DOI: 10.1124/mol.119.118448
This article has not been copyedited and formatted. The final version may differ from this version.



Yang S, Edman LC, Sánchez-Alcañiz JA, Fritz N, Bonilla S, Hecht J, Uhlén P, Pleasure SJ, Villaescusa JC, Marín O, and Arenas E (2013) CXCL12/CXCR4 signaling controls the migration and process orientation of A9-A10 dopaminergic neurons. *Development* **140:** 4554-64.

Zhang XC, Liu J, and Jiang D (2014) Why is dimerization essential for class-C GPCR function? New insights from mGluR1 crystal structure analysis. *Protein Cell* **5:** 492-495.

Zhao H, Guo L, Zhao H, Zhao J, Weng H, and Zhao B (2015) CXCR4 over-expression and survival in cancer: a system review and meta-analysis. *Oncotarget* **6:** 5022-5040.

Ziegler N, Bätz J, Zabel U, Lohse MJ, and Hoffmann C (2011) FRET-based sensors for the human M1, M3-, and M5-acetylcholine receptors. *Bioorg Med Chem* **19:** 1048-1054.

Molecular Pharmacology Fast Forward. Published on May 30, 2020 as DOI: 10.1124/mol.119.118448
This article has not been copyedited and formatted. The final version may differ from this version.



**Footnotes**

This work was supported by the European Union's Horizon 2020 Program under grant agreement 641833 (Oncornet); the Deutsche Forschungsgemeinschaft [Grant TR166 ReceptorLight project C02]; and the Medical Research Council [MR/N020081/1].

Molecular Pharmacology Fast Forward. Published on May 30, 2020 as DOI: 10.1124/mol.119.118448
This article has not been copyedited and formatted. The final version may differ from this version.



**Figure legends**

**Figure 1. Principle and functional characterization of the CXCR4-FlAsH228-CFP sensor. (A)** Schematic depicting the intramolecular FRET-based sensor. Ligand-induced conformational changes in CXCR4 are monitored as changes in FRET. **(B)** Representative confocal images of HEK293 cells transiently expressing CXCR4-FlAsH228-CFP and FlAsH-labeled prior to the measurement. Upper panel shows CFP emission. Lower panel shows FlAsH emission. Scale bar denotes 10 µm. **(C)** Intramolecular FRET efficiency of CXCR4-FlAsH228-CFP as determined by BAL treatment. Values were calculated from the increase in the CFP fluorescence upon BAL addition. Data shows mean ± SD of 20 cells measured on 4 independent experimental days. A representative individual experiment is shown in Figure S2. **(D)** $G_{i1}$ activation via CXCR4 or CXCR4-FlAsH228 in response to increasing concentrations of CXCL12. Data show mean ± SEM and are representative of n=3 independent experiments conducted in quadruplicate. In this particular experiment, $EC_{50}$=3.3 and 14.7 nM for CXCR4 and CXCR4-FlAsH228, respectively. **(E)** Inhibition of FSK-induced cAMP accumulation in response to increasing concentrations of CXCL12 by HEK293T cells expressing CXCR4, CXCR4-CFP, or CXCR4-FlAsH228-CFP. Data show mean ± SEM and are representative of n=4 independent experiments conducted in triplicate. In this particular experiment, $EC_{50}$=7.3, 11.3, and 39.0 nM for CXCR4, CXCR4-CFP, and CXCR4-FlAsH228-CFP, respectively. Characterization of the CXCR4-FlAsH226-CFP and CXCR4-FlAsH229-CFP sensors is presented in Figure S1.

**Figure 2. The CXCR4-FlAsH228-CFP sensor reports the dynamics and kinetics of receptor activation and deactivation. (A, B)** Representative traces of the FRET response from a single HEK293 cell expressing the CXCR4-FlAsH228-CFP sensor and stimulated with 30 µM CXCL12 for the indicated period of time (black line). Left panel shows corrected and normalized FRET ratio. Right panel shows corrected FlAsH (yellow) and CFP (cyan) emissions. **(C)** Kinetic analysis of receptor activation. The FRET change was fitted to a one component exponential decay function to obtain the time constant τ. **(D, E)** On-kinetics of CXCR4 in response to CXCL12 (D) and off-kinetics of CXCR4 upon wash-out of the ligand with buffer (E). Tau values from individual experiments are represented in a scatter plot. Data show median and IQR of 17 cells measured on 4 independent experimental days.

Molecular Pharmacology Fast Forward. Published on May 30, 2020 as DOI: 10.1124/mol.119.118448
This article has not been copyedited and formatted. The final version may differ from this version.



**Figure 3. CXCL12 induces rearrangements between CXCR4 and the $G_{i1}$ protein. (A, B)** Schematic depicting the settings employed to investigate the interaction between the receptor and the $G_{i1}$ protein. HEK293 cells were transfected with CXCR4-YFP and $G\alpha_{i1}/G\beta_1/G\gamma_2$-CFP (A) or $G\alpha_{i1}$-CFP/$G\beta_1/G\gamma_2$ (B). **(C, D)** Representative traces of the FRET response from a single HEK293 cell expressing CXCR4-YFP and the G protein CFP-labeled at the $G\gamma_2$ (C) or $G\alpha_{i1}$ subunit (D) and stimulated with 30 μM CXCL12 for the indicated period of time (black line). Upper panels show corrected YFP (yellow) and CFP (cyan) emissions. Lower panels show corrected and normalized FRET ratios. **(E)** On-kinetics of the interaction of CXCR4 with the $G_{i1}$ protein upon CXCL12 stimulation as measured in the two settings. Tau values from individual experiments are represented in a scatter plot. Data show median and IQR of 12 cells for each setting, measured on at least 3 independent experimental days. Statistical significance was tested using Mann-Whitney test (n.s.=non-significant).

**Figure 4. CXCR4 resides within FRET distance from $G_i$ proteins in the absence of agonist. (A)** Schematic of acceptor photobleaching experiments. Donor and acceptor emissions were measured prior to and after photobleaching the YFP in HEK293 cells expressing the constructs $G\alpha_{i1}/G\beta_1/G\gamma_2$-CFP and $\alpha_{2A}$-AR-YFP or CXCR4-YFP. The latter was also measured in the presence of IT1t. **(B)** The change in the CFP fluorescence ($F_{CFP}$) after YFP photobleaching from individual experiments in each condition is shown as a box plot. N=19, 13, and 12 cells for CXCR4, CXCR4 + IT1t, and $\alpha_{2A}$-AR, respectively, measured on 3 independent experimental days. Statistical significance was tested using unpaired t-test (***$p \leq 0.001$; ****$p \leq 0.0001$). **(C-E)** Representative CFP (cyan) and YFP (yellow) traces from individual experiments. The YFP photobleaching period is indicated in grey.

**Figure 5. CXCR4 activates $G_i$ proteins in response to CXCL12. (A)** FRET-based sensors for $G_{i1}$, $G_{i2}$, $G_{i3}$, and $G_q$ were employed to study G protein activation. A loss of FRET between the Gγ-Venus and Gα-mTurquoise2 subunits is detected upon activation. **(B-C)** Representative traces of the FRET response from a single HEK293 cell expressing the $G_{i2}$ sensor and CXCR4 (B) or $\alpha_{2A}$-AR (C) and

Molecular Pharmacology Fast Forward. Published on May 30, 2020 as DOI: 10.1124/mol.119.118448
This article has not been copyedited and formatted. The final version may differ from this version.



stimulated with 30 μM CXCL12 or 100 μM norepinephrine, respectively (black line). Upper panels show corrected Venus (yellow) and mTurquoise2 (cyan) emissions. Lower panels show corrected and normalized FRET ratios. Figure S3 shows activation of $G_{i1}$ and $G_{i3}$. **(D)** Kinetics of $G_{i1}$, $G_{i2}$, and $G_{i3}$ protein activation via CXCR4 or $\alpha_{2A}$-AR in response to CXCL12 and norepinephrine, respectively. Table shows median and IQR. Tau values from individual experiments are represented in a scatter plot with median and IQR. For CXCR4, n=11, 22 and 11 cells for $G_{i1}$, $G_{i2}$ and $G_{i3}$ activation, respectively, measured on at least 3 independent experimental days. For $\alpha_{2A}$-AR, n=17, 16 and 7 cells for $G_{i1}$, $G_{i2}$ and $G_{i3}$ activation, respectively, measured on at least 2 independent experimental days. Statistical significance was tested using Kruskal-Wallis test (n.s.=non-significant)**. (E)** CXCR4-mediated activation of $G_{i1}$, $G_{i2}$, $G_{i3}$, and $G_q$ activation in response to increasing concentrations of CXCL12. As a control, empty plasmid was transfected instead of receptor. Data show mean ± SEM and are representative of n=5 independent experiments conducted in quadruplicate. In this particular experiment, $EC_{50}$ values were 9.7, 10.8, and 17.1 nM for $G_{i1}$, $G_{i2}$ and $G_{i3}$, respectively. **(F)** FRET of cells expressing the CXCR4 and $G_{i2}$ sensor upon treatment with buffer, buffer supplemented with 100 μM IT1t or 100 nM CXCL12. Data are representative of 3 independent experiments. Data shows mean ± SD and is normalized to buffer treatment. N=30, 30, and 15 wells (containing 15,000 cells each) for the treatment with buffer, IT1t and CXCL12, respectively. Statistical significance was tested using unpaired t-test (**$p \leq 0.01$; ****$p \leq 0.0001$).

**Figure 6. CXCR4 homodimers undergo conformational changes in response to CXCL12. (A)** The rearrangement between CXCR4 protomers was investigated in HEK293 cells co-transfected with CXCR4-CFP and CXCR4-YFP, with the fluorophores fused to the C-termini. **(B)** Representative traces of the FRET response from a single HEK293 cell expressing CXCR4-YFP and CXCR4-CFP and stimulated with 30 μM CXCL12 (black line). Upper panel shows corrected YFP (yellow) and CFP (cyan) emissions. Lower panel shows corrected and normalized FRET ratio. **(C-D)** On-kinetics of the rearrangement between CXCR4 protomers in response to CXCL12 (C) and off-kinetics upon wash-out of the ligand with buffer (D). Tau values from individual experiments are represented in a scatter plot with median and IQR. N=28 and 10 cells, respectively, measured on 4 independent experimental days.

Molecular Pharmacology Fast Forward. Published on May 30, 2020 as DOI: 10.1124/mol.119.118448
This article has not been copyedited and formatted. The final version may differ from this version.



**Figure 7. MIF induces structural rearrangements in CXCR4 but does not lead to $G_i$ protein activation. (A, C, E, G)** Representative traces of the FRET response from a single HEK293 cell transiently expressing: CXCR4-FlAsH228-CFP sensor (A), CXCR4-YFP and $G\alpha_{i1}/G\beta_1/G\gamma_2$-CFP (C), CXCR4-CFP and CXCR4-YFP (E) or CXCR4 and $G_{i2}$ sensor (G), and stimulated with 100 μM MIF, followed by wash-out and then stimulation with 30 μM CXCL12. Upper panels show corrected acceptor (yellow) and donor (cyan) emissions. Lower panels show corrected and normalized FRET ratios. **(B, D, F)** On-kinetics of receptor activation (n=9 cells) (B), receptor/G protein interaction (n=13 cells) (D) and rearrangement between CXCR4 protomers (n=17 cells) (F) in response to 100 μM MIF. Tau values from individual experiments are represented in a scatter plot with median and IQR. Measurements were performed on at least 2 independent experimental days. **(H)** Comparison of CXCR4 on-kinetics in response to CXCL12 and MIF. Data from receptor activation belongs to Figures 2D and 7B. Data from receptor/G protein interaction belongs to Figures 3E (Gγ-labeled) and 7D. Data from protomers rearrangement belongs to Figures 6C and 7F. Data from G protein activation belongs to Figure 5D ($G_{i2}$ sensor). Data are shown as a box plot in which the whiskers represent maximum and minimum values.

**Figure 8. Summary of the findings in this manuscript regarding the CXCL12/CXCR4 axis.** The upper part of the figure shows the kinetics of each step of the signaling cascade investigated using FRET. The main findings regarding the CXCL12/CXCR4 axis are: 1) Activation kinetics of CXCR4 upon CXCL12 binding are slower than other class A GPCRs. 2) Rearrangements within dimers occur faster than activation of $G_i$ proteins. 3) This axis leads to a prolonged activation of $G_i$ proteins. 4) CXCR4 exhibits some degree of constitutive activity. It is tempting to speculate that the rearrangement between protomers precedes G protein activation which might suggest that conformational changes in CXCR4 homodimers, when present, play a possible role in the signaling activation course of this receptor as depicted in model B. However, we need to emphasize that mechanistic interpretation needs to be based on measuring microscopic rate constants and hence

Molecular Pharmacology Fast Forward. Published on May 30, 2020 as DOI: 10.1124/mol.119.118448
This article has not been copyedited and formatted. The final version may differ from this version.



model A, where the dimer rearrangement offers an alternative pathway, is also compatible with our dataset.

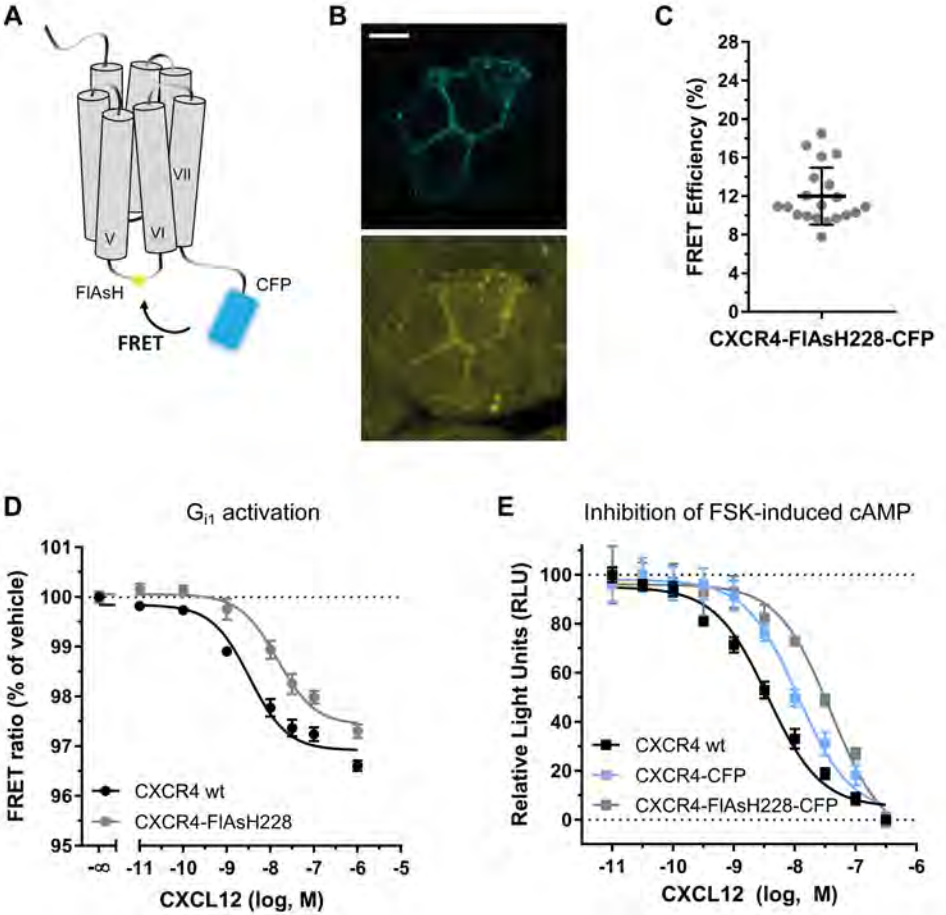
A
VII
V
VI
FlAsH
CFP
FRET
B
C
FRET Efficiency (%)
28
24
20
16
12
8
4
0
CXCR4-FlAsH228-CFP
D
$G_{i1}$ activation
FRET ratio (% of vehicle)
101
100
99
98
97
96
95
CXCR4 wt
CXCR4-FlAsH228
-∞
-11
-10
-9
-8
-7
-6
-5
CXCL12 (log, M)
E
Inhibition of FSK-induced cAMP
Relative Light Units (RLU)
100
80
60
40
20
0
CXCR4 wt
CXCR4-CFP
CXCR4-FlAsH228-CFP
-11
-10
-9
-8
-7
-6
CXCL12 (log, M)

**Figure 1**

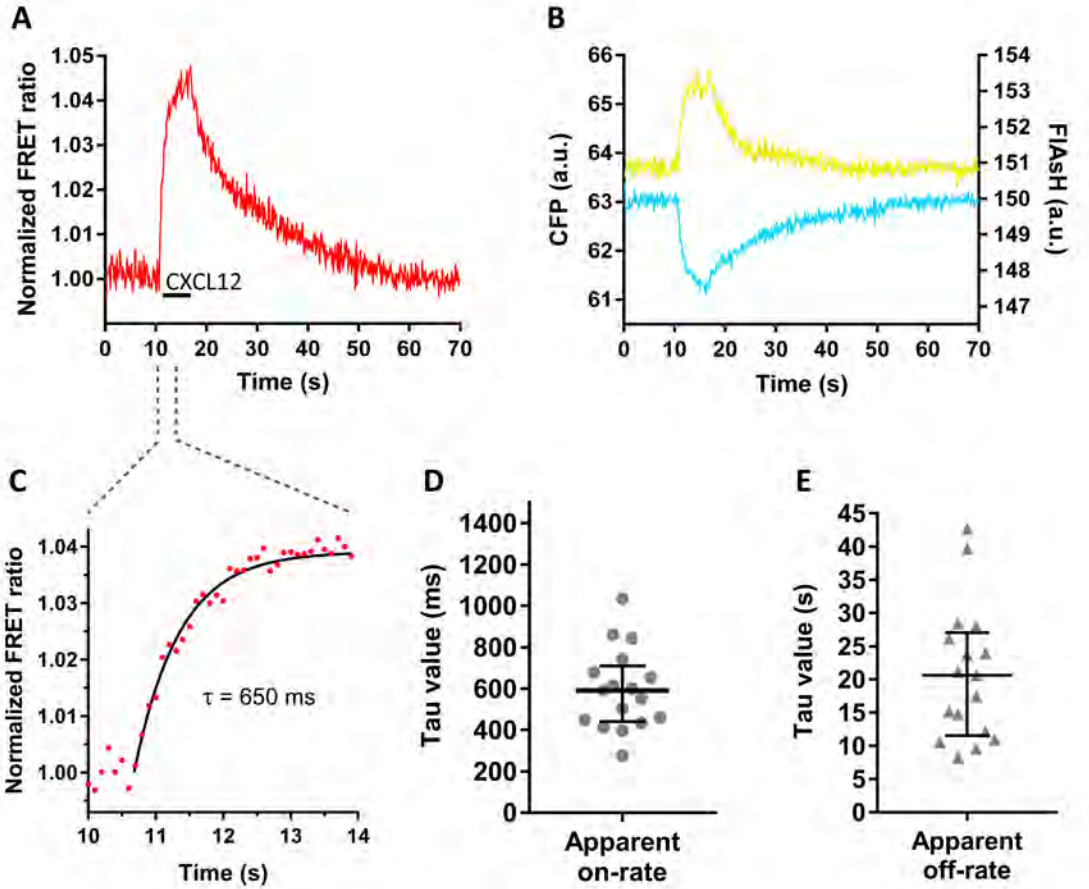
A
Normalized FRET ratio
1.05
1.04
1.03
1.02
1.01
1.00
CXCL12
0 10 20 30 40 50 60 70
Time (s)
B
CFP (a.u.)
66
65
64
63
62
61
FlAsH (a.u.)
154
153
152
151
150
149
148
147
0 10 20 30 40 50 60 70
Time (s)
C
Normalized FRET ratio
1.04
1.03
1.02
1.01
1.00
τ = 650 ms
10 11 12 13 14
Time (s)
D
Tau value (ms)
1400
1200
1000
800
600
400
200
0
Apparent on-rate
E
Tau value (s)
45
40
35
30
25
20
15
10
5
0
Apparent off-rate

Figure 2

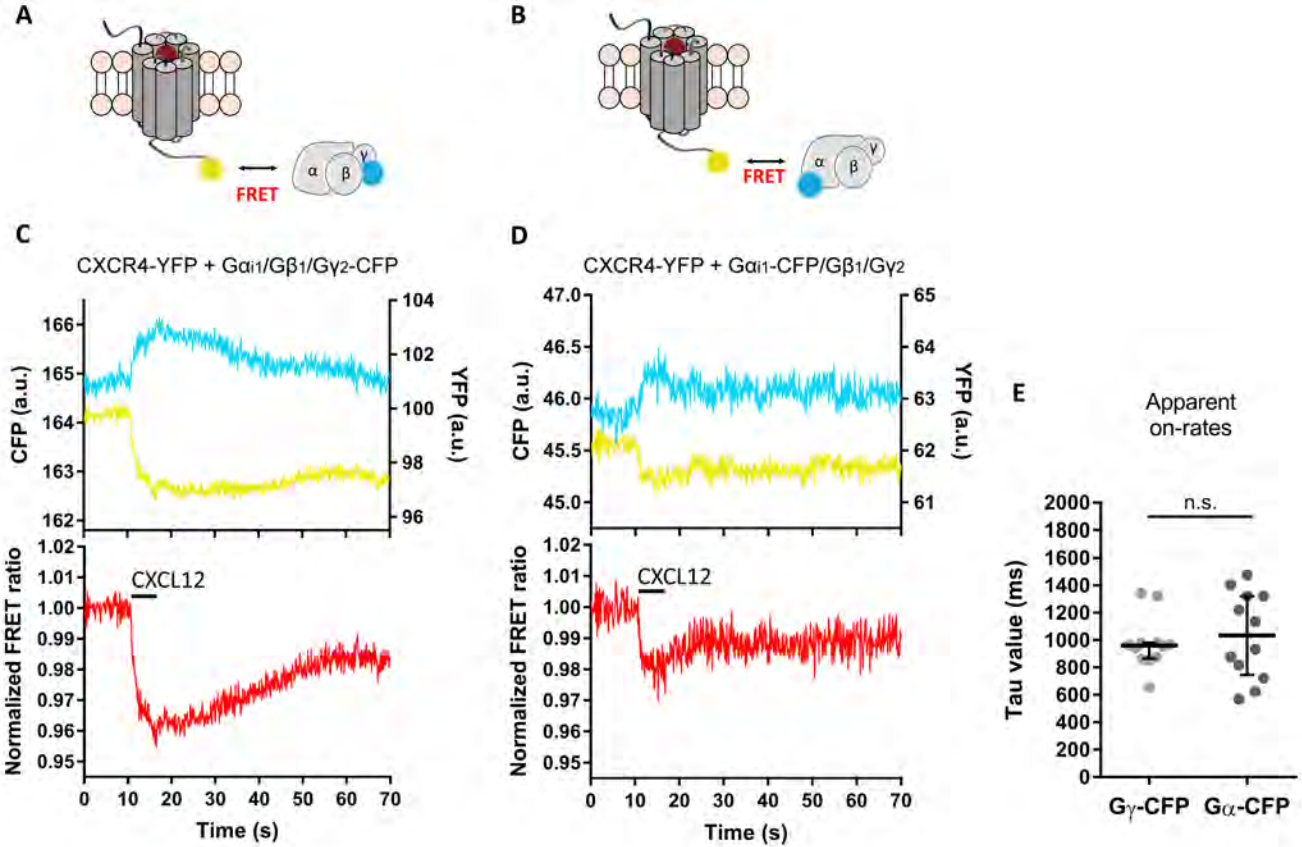
A
FRET
α
β
γ
B
FRET
α
β
γ
C
CXCR4-YFP + Gαi1/Gβ1/Gγ2-CFP
CFP (a.u.)
YFP (a.u.)
Normalized FRET ratio
CXCL12
Time (s)
D
CXCR4-YFP + Gαi1-CFP/Gβ1/Gγ2
CFP (a.u.)
YFP (a.u.)
Normalized FRET ratio
CXCL12
Time (s)
E
Apparent on-rates
n.s.
Tau value (ms)
Gγ-CFP
Gα-CFP

**Figure 3**

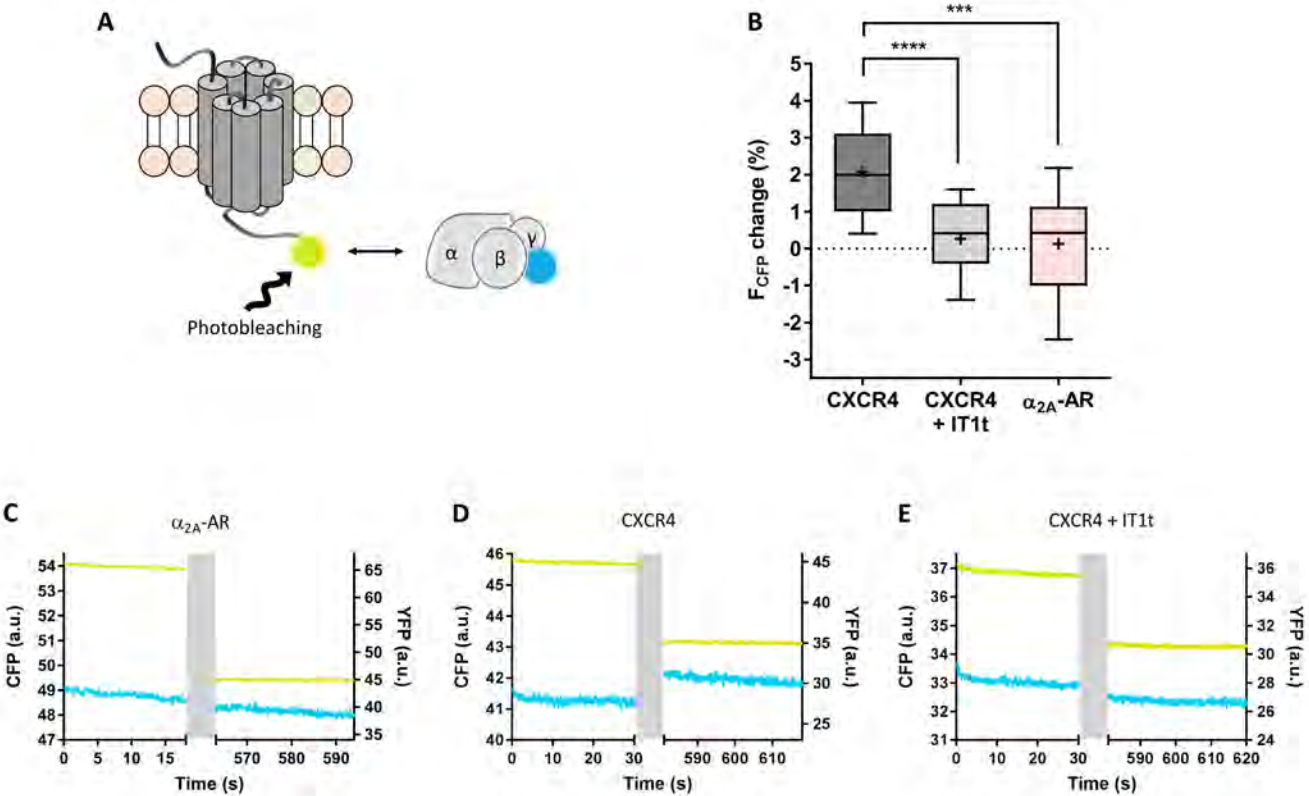
A
Photobleaching
α
β
γ
B
***
****
$F_{CFP}$ change (%)
CXCR4
CXCR4 + IT1t
$\alpha_{2A}$-AR
C
$\alpha_{2A}$-AR
CFP (a.u.)
YFP (a.u.)
Time (s)
D
CXCR4
CFP (a.u.)
YFP (a.u.)
Time (s)
E
CXCR4 + IT1t
CFP (a.u.)
YFP (a.u.)
Time (s)

**Figure 4**

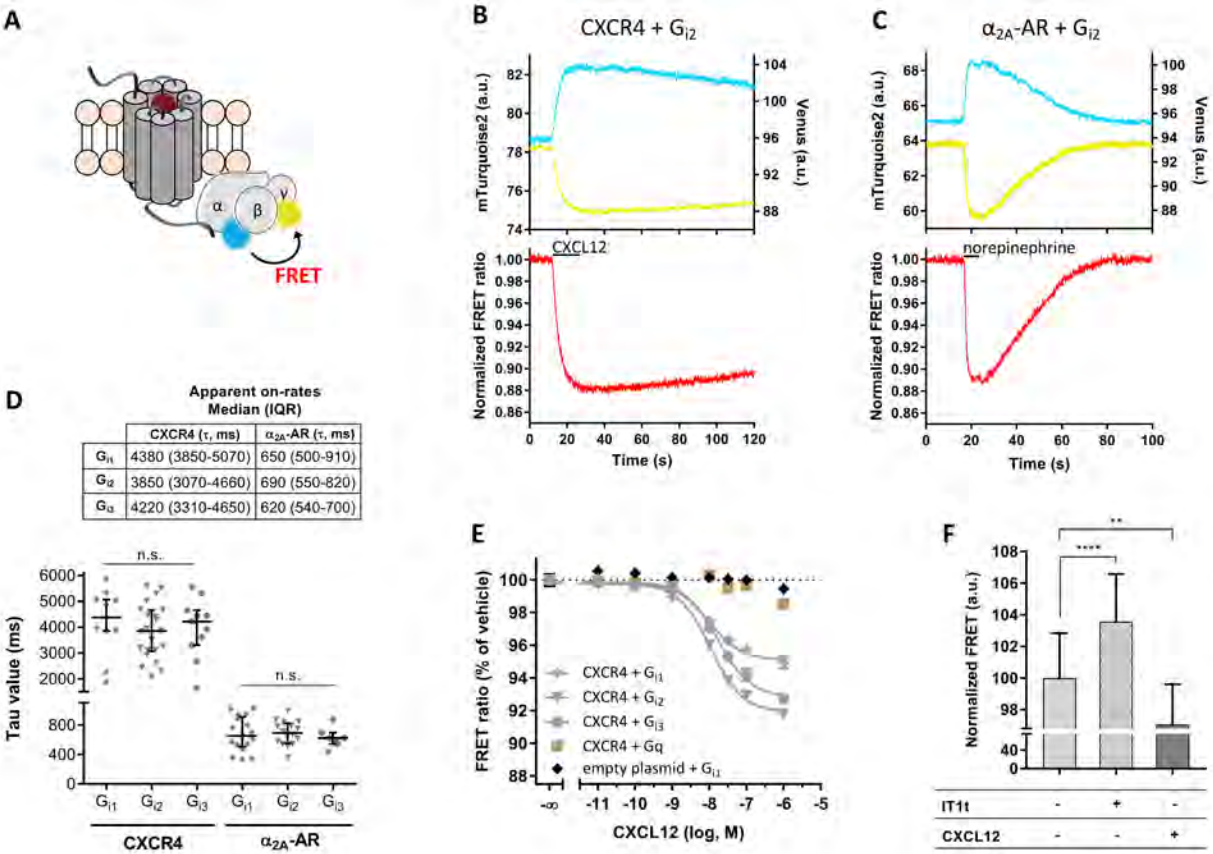


| | CXCR4 (τ, ms) | $\alpha_{2A}$-AR (τ, ms) |
|---|---|---|
| $G_{i1}$ | 4380 (3850-5070) | 650 (500-910) |
| $G_{i2}$ | 3850 (3070-4660) | 690 (550-820) |
| $G_{i3}$ | 4220 (3310-4650) | 620 (540-700) |

**Figure 5**

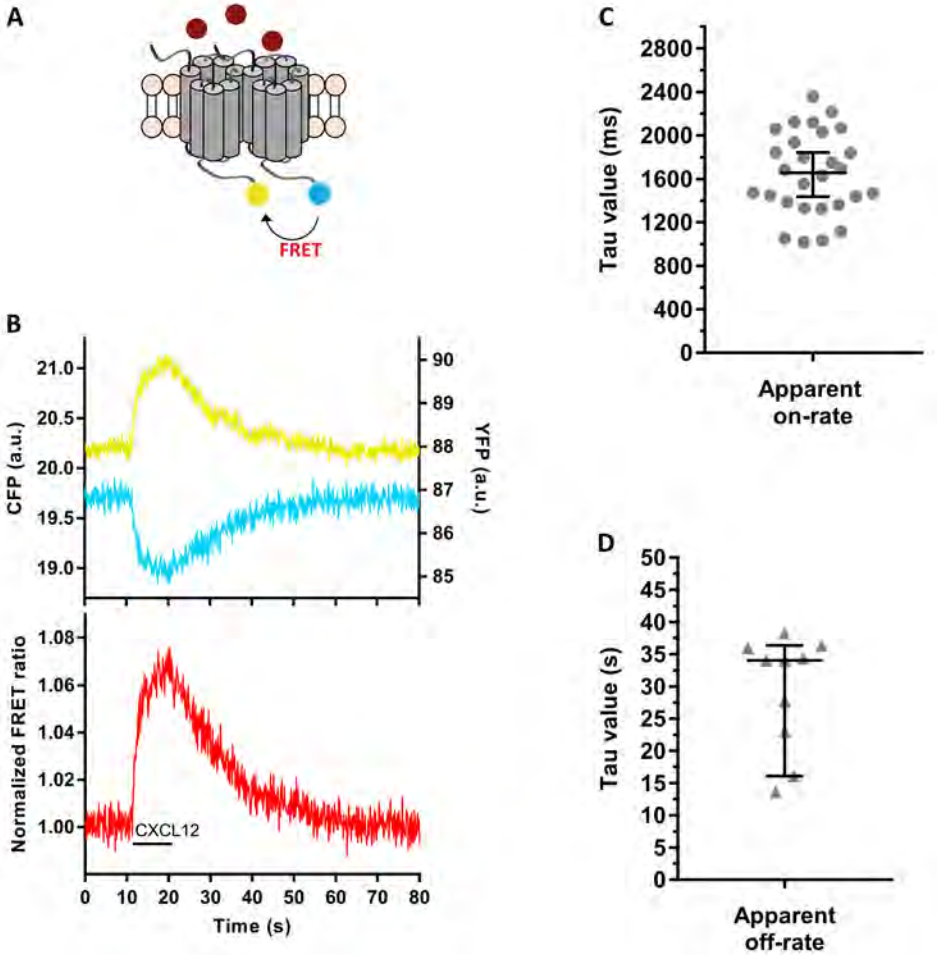
A
FRET
B
CFP (a.u.)
YFP (a.u.)
Normalized FRET ratio
CXCL12
Time (s)
C
Tau value (ms)
Apparent on-rate
D
Tau value (s)
Apparent off-rate

Figure 6

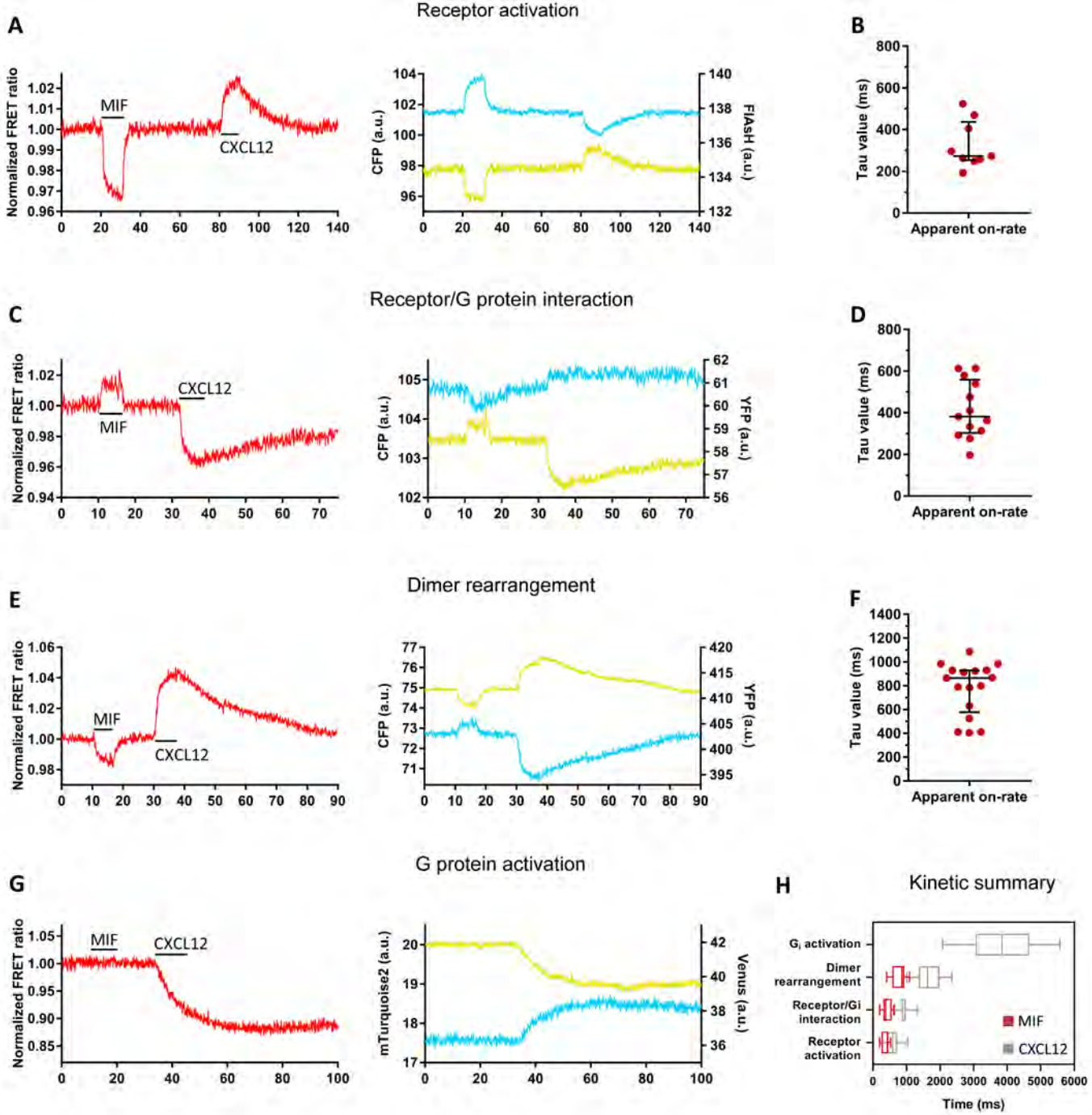
A
Receptor activation
Normalized FRET ratio
MIF
CXCL12
CFP (a.u.)
FlAsH (a.u.)
B
Tau value (ms)
Apparent on-rate
C
Receptor/G protein interaction
Normalized FRET ratio
MIF
CXCL12
CFP (a.u.)
YFP (a.u.)
D
Tau value (ms)
Apparent on-rate
E
Dimer rearrangement
Normalized FRET ratio
MIF
CXCL12
CFP (a.u.)
YFP (a.u.)
F
Tau value (ms)
Apparent on-rate
G
G protein activation
Normalized FRET ratio
MIF
CXCL12
mTurquoise2 (a.u.)
Venus (a.u.)
H
Kinetic summary
Gi activation
Dimer rearrangement
Receptor/Gi interaction
Receptor activation
MIF
CXCL12
Time (ms)

**Figure 7**